Äspö Hard Rock Laboratory

Numerical modelling of discontinuities to study the effect on the state of stress

Beatrice Lundholm

Luleå University of Technology

November 2000

SKB

**Äspö Hard Rock
Laboratory**

Äspö Hard Rock Laboratory

Numerical modelling of discontinuities to study the effect on the state of stress

Beatrice Lundholm

Luleå University of Technology

November 2000

Foreword

The research work presented in this report was carried out from June 1999 to April 2000.

Luleå November 2000

Beatrice Lundholm

Abstract

The project, of which the second part is presented in this report, consists of two parts. The first part was to define the state of stress at Äspö Hard Rock Laboratory and this has been reported in " Rock stress and Rock Stress Measurements at Äspö". In this second part, investigations of the correlation between the stress and geological structures are made, using numerical modelling tools as FLAC, UDEC and 3DEC.

The 2D-modelling in FLAC was made to simulate the overcoring and biaxial testing. The result show that it is possible to obtained extensional strain in the core during overcoring if the major principal stress is perpendicular to the borehole axis. This may lead to microcracking occurring in the core causing high Poisson's ratio, which results in higher stresses. It can also be seen from the simulation of the biaxial testing that extensional strain is achieved even if the hollow core is not damaged during overcoring.

The analyses using UDEC was made to study the effect of different properties of a discontinuity, such as the dip angle, Young's modulus, Poisson's ratio, density and the normal and shear stiffness in 2D-models. The analyses showed that an inclined discontinuity affects the stresses especially if sliding occurs. So, the dip angle does not solely, determine the amount of disturbance of the state of stress around a discontinuity. If slip will occur or not depends, thus, on a combination of dip angle, friction angle and the far field state of stress. A dip angle of 30 degrees affected the major principal stress most, while the minor principal stress is most affected by a dip angle of 45 degrees, for a friction angle of $10°$. The results from the simulation of a thick zone showed that the elastic properties of the zone material mainly affect the stresses within the zone. However, higher values of Young's modulus and Poisson's ratio in the zone than in the side rock resulted in higher stresses within the zone than outside. The orientation of the major principal stress becomes more perpendicular to the zone.

The 3-dimensional analyses using 3DEC was made in order to investigate if the stresses at Äspö could be correlated with the major geological structures. The results show that the increase in the horizontal stress seen both in KAS02 and KAS03 is obtained in the model when using a bilinear stress state that is based on the measurements performed at Äspö. However, a satisfying coincidence is not obtained with the measured stresses in KAS02, KAS03, KAS05 and KZXSD8HL, which were the boreholes used as reference boreholes. One of the reasons for the disagreement may mainly be that the discontinuities used in the 3DEC model are more or less vertical. The least dip angle used is 60 degrees. Another reason may be that the measured stresses are influenced by far more parameters than are used in the 3DEC-model, such as different rock types, smaller discontinuities and mineral grains.

Sammanfattning

Projektet, av vilket den andra delen presenteras i denna rapport, består av två delar. Den första delen bestod i att bestämma spänningstillståndet kring Äspö Hard Rock Laboratory, vilket har blivit redovisat i "Rock Stress and Rock Stress Measurements at Äspö". I denna andra och sista del, studeras kopplingen mellan spänningar och geologiska strukturer genom att använda numeriska beräkningsprogram som FLAC, UDEC samt 3DEC.

Genom de tvådimensionella analyserna i FLAC simulerades överborrningen och biaxial testet, för att studera hur de påverkade bergprovet. Resultaten visade att dragtöjningar i kärnan uppstår vid överborrningen när den största huvudspänningen är vinkelrät mot borrhålsaxeln. Detta kan leda till att mikrosprickor bildas i provet, vilket i sin tur kan resultera i högre Poisson's tal än vad som gäller egentligen för bergprovet. Genom att spänningen är direkt proportionell mot Poisson's tal leder ett högt Poissan's tal till högre spänningar än förväntat. Simuleringen av biaxialtestet visar också att dragtöjningar bildas i kärnan även om den var helt opåverkad av överborrningen.

För att 2D analysera hur olika egenskaper hos en spricka, så som stupning, sprickfyllnadsmaterialets elasticitetsmodul, Poisson's tal och densiteten samt normal- och skjuvstyvheten hos sprickytan, påverkar spänningarna har UDEC används.

Resultaten visade att en lutande spricka påverkar spänningen speciellt då glidning inträffar. Med andra ord så påverkar inte spänningstillståndet in närheten av en spricka enbart på stupningen på sprickan. Om glidning inträffar eller inte beror således på en kombination av stupningen, friktionsvinkeln samt ursprungligt spänningstillstånd. Då friktionsvinkeln på sprickplanet är 10 grader, påverkas den största huvudspännigna mest när stupningsvinkeln är 30 grader, medan den minsta huvudspänningen på verkas av en spricka med stupning 45 grader. Analyserna av hur elasticitetsmodulen, Poisson's tal och densitet på material i zonen påverkar spänningarna visade att spänningarna i den närliggande bergmassan endast på verkades då kontaken mellan zon och omgivande berg hade låg hållfasthet. Då kontakterna gavs hög hållfasthet påverkas endast spänningarna i själva zonen Det senare fallet visade också att då högre värden på elasticitetsmodulen och Poisson's tal gavs på zonmaterialet än på omgivande bergmassa, blev spänningarna i zonen högre än i omgivande berg samt att orienteringen av den största huvudspänningen blev mer eller mindre vinkelrät zonen.

Syftet med den 3-dimensionella analysen i 3DEC var att studera ifall spänningarna på Äspö kunde korreleras de dominerande geologiska strukturerna. Resultaten visar att ökning i de horisontella spänningarna som är tydlig i KAS02 och KAS03 erhålles då ett bilinjärt spänningsfält baserat på tidigare bergspänningsmätningar på Äspö används som randspänningar. Emellertid, är inte korrelationen med de uppmätta spänningarna i KAS02, KAS03, KAS05 och KZXSD8HL som vilka borrhål har används som referens borrhål helt tillfredställande. En av orsakerna till detta kan vara att sprickorna i 3DEC modellen är mer eller mindre vertikala, den minsta stupningen är 60 grader. Ytterligare orsak kan vara att de uppmätta spänningarna är påverkade av en rad fler egenskaper än vad som är medtagit i 3DEC, t ex flera olika bergarter, mindre sprickor och mineralkorn i mätpunkten.

Contents

List of Figures

List of Tables

1 Introduction

1.1 Definition of rock stresses

Rock stresses can be divided into *in situ* stresses and induced stresses. *In situ* stresses are called natural, primitive or virgin stresses and exist in the rock prior to any disturbance. Induced stresses are related to artificial disturbance (excavation, drilling, pumping). These stresses can also be induced by changing of natural conditions (swelling, drying etc.).

The current *in situ* stresses in a rock mass are the cumulative product of events in the geological history. Several authors have proposed different terminology for *in situ* stress, which are summarised by Amadei and Stephansson (1997). The *in situ* stresses can be divided into four groups of origin; gravitational, tectonic, residual and terrestrial stresses (Figure 1-1).
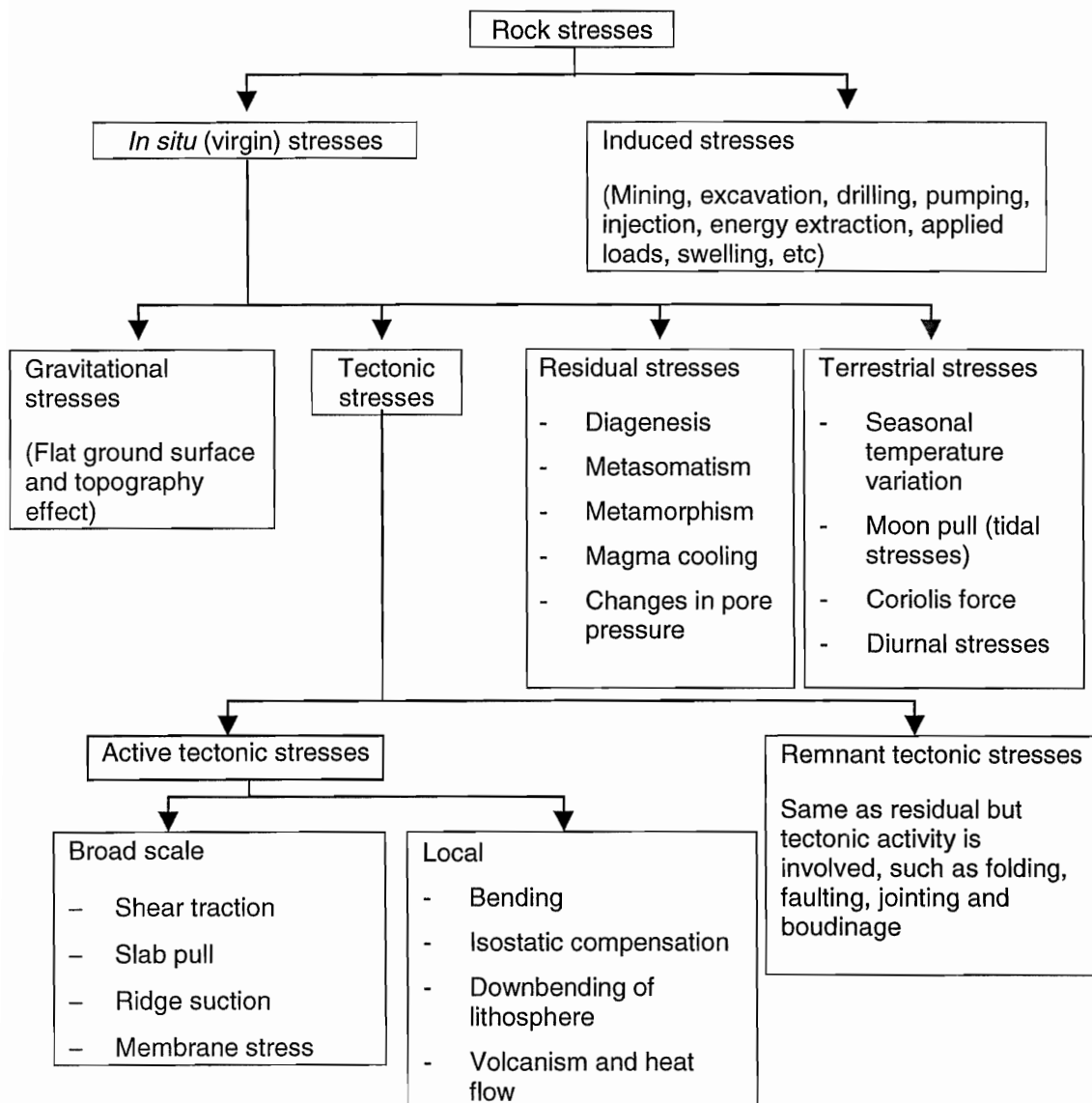
Figure 1-1   *Terminology of rock stresses (Amadei and Stephansson, 1997).*

The definition of induced stresses is that they are stress changes due to removal or addition of material. These induced stress changes are superimposed on the natural stresses that exist before the excavation. The result of this superposition will be named secondary rock stresses, whereas the *in situ* stresses will be named virgin stresses in this report.

1.2 Rock stress versus geology

The assumption in rock stress measurements is that the rock is a continuous, homogeneous, isotropic and linearly elastic material and that its behaviour is not changing over time. These assumptions have been analysed in more detail by Hudson and Cooling (1988) and will be presented in the following.

On a large scale the rock is not continuous and the stress field can be altered by discontinuities in the rock mass. Discontinuities are one of the most severe local perturbations to the overall stress field. In the paper by Hudson and Cooling (1988) the behaviour of the major principal stress near a discontinuity is discussed, see Figure 1-2.

If the discontinuity is open, the major principal stress turns to be parallel to the discontinuity. If the discontinuity is filled with material, which has the same properties as the surrounding rock, the principal stresses may be unaffected. On the other hand, if the material in the discontinuity is stiffer, i.e. Young's modulus is higher than for the surrounding rock, the major principal stress turns to be perpendicular to the discontinuity.
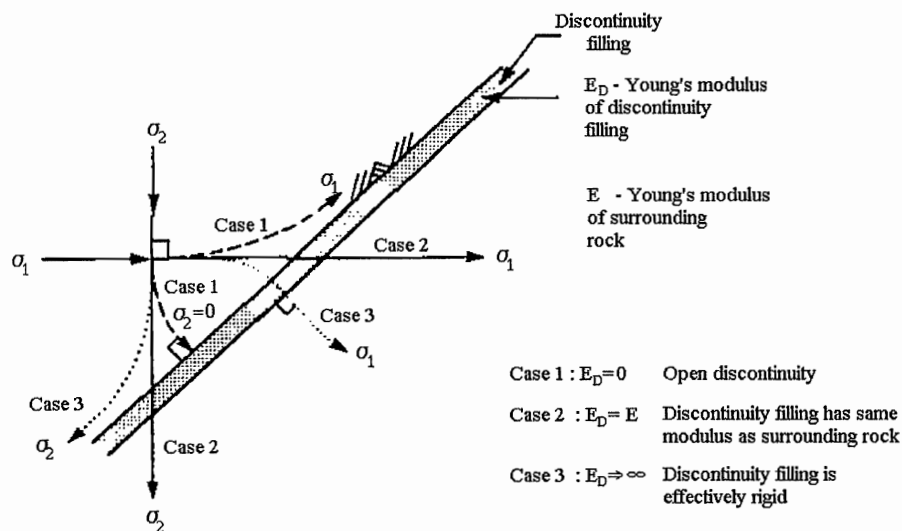
Figure 1-2   The effect of a discontinuity on the stress state (Hudson and Cooling, 1988).

The stress field perturbation could be on a very large or a very small scale, depending on the type of the discontinuity, i.e. faults, joints, fissures or microfissures and also on the properties of the discontinuity. For example, the vertical stress can vary considerably along a line through the rock mass, as illustrated in Figure 1-3.
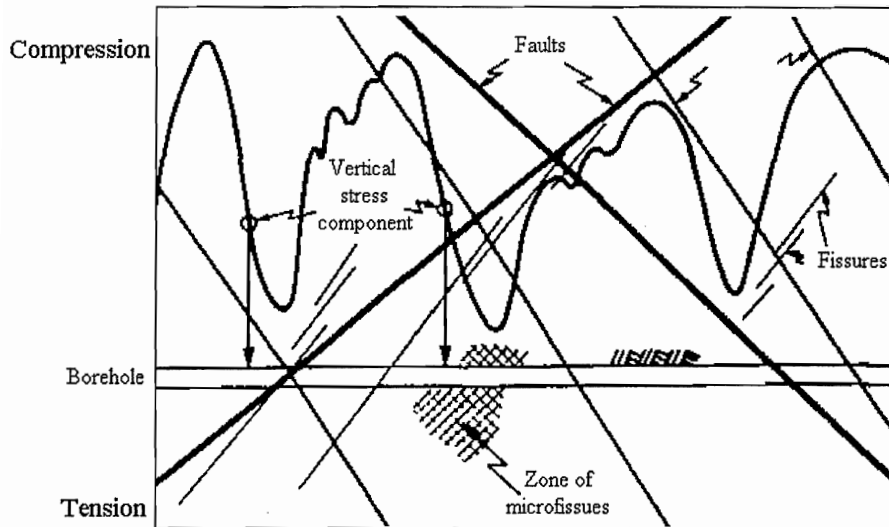
Figure 1-3 *Vertical cross-section through an idealised rock mass with the possible variation in the vertical stress component (Hudson and Cooling, 1988).*

Since the mechanical properties of the intact rock vary much in the rock mass the stresses will be even more scattered in the rock mass. For instance, the stress tends to be higher where the rock is stiffer (Hudson and Cooling, 1988).

Contrary to the common assumptions, used in stress measurements the rock may not be isotropic and linearly elastic. This affects the accuracy of the rock stress measurements and furthermore it may make the data reduction methods based on linear elasticity invalid. However, more recent investigations have been made to establish evaluation models with respect to the anisotropy in the rock mass (Amadei and Stephansson, 1997).

The rock behaviour may be time dependent. The virgin stress may have been in a state of equilibrium over a geological time. However, the state of the stress may still be changing during a stress measurement programme, due to induced stresses caused by excavation.

1.2.1   Discontinuities

In rock mechanics, several names are used to denote a discontinuity in the rock mass. In this report following definition and names are used.

− A microcrack has usually a length of micrometres to centimetres

− A joint is up to a metre

− Larger joints are larger than a metre.

In this report the effect of the large discontinuities on the local state o stress as well as the small microcracks that may effect the results during stress measurements using overcoring technique will be studied. These microcracks may be natural or induced during overcoring or during biaxial testing.

3

1.3 Numerical modelling

In order to study the effect of the major geological structures at Äspö on the stress state numerical analyses have been used as a tool. During this work, three types of numerical programs have been used, **U**niversal **D**istinct **E**lement **C**ode, UDEC version 3.0, **T**hree **D**imensional **E**lement **C**ode, 3DEC version 2.1 and **F**ast **L**agrangian **A**nalysis of **C**ontinua, FLAC version 3.4 (Itasca Consulting Group, 1998). All programs are command-driven codes based on distinct element method (UDEC, 3DEC) and finite difference method (FLAC).

The effects of a single discontinuity, a single discontinuity zone and the stiffness of a discontinuity have been studied using generic models and UDEC.

These models have been used mainly to investigate how different parameters such as dip angle of the discontinuity, stiffness, the elastic properties and the density of the material in the discontinuity affect the stress distribution. The results from those analyses have then been used to build a three-dimensional model. In the 3D model the influence of the major geological structures at Äspö on the local state of stress was studied using 3DEC.

FLAC has been used to investigate how the core is affected by the overcoring during rock stress measurements and during the biaxial testing. FLAC was used since the program has a pre-defined function called axi-symmetrical model that made it possible to study a 3D problem in 2D.

When using numerical analyses as a tool there are several reasons for not making a too detailed model due to the geological structures. The main arguments are (UDEC version 3.0):

1. it is futile to ever expect to have sufficient data to model a jointed rock mass in every detail.

2. the memory of a computer is limited.

3. too many details involved in a model make it difficult to interpret the simulation results, particularly in sensitivity studies.

The modelling is conducted in a specific manner. First, the model is run with the true elastic properties of the rock mass and the discontinuities and high strength values to consolidate the model. Then for each analysis, the current strength properties are changed to relevant values and the model is run to equilibrium. The process to equilibrium is monitored by a number of history points, which are reflecting the changes of the stresses, displacements and velocities in some points.

1.4 Objectives

This report is the second of two reports, which have been done for a licentiate thesis at the Division of Rock Mechanics, Luleå University of Technology. The main objectives of the project are

– to establish the state of the stress at Äspö

– to correlate rock stresses with the major geological structures at Äspö

– to investigate the reliability of the measuring data

4

The first part was to define the state of the stresses at Äspö Hard Rock Laboratory. This was done based on earlier rock stress measurements conducted during the years 1988 to 1997. Two different measurement techniques have been used, hydraulic fracturing and overcoring. For the overcoring techniques two types of cells were used, CSIRO HI-cell and a cell developed by the Swedish State Power Board (SSPB). This part was presented in the first report "Rock stress and rock stress measurements at Äspö HRL" (Lundholm, 2000). An outcome from this report was that the Young's modulus and especially the Poisson's ratio showed different values depending on the overcoring cell that was used. This raised the idea that the elastic properties of the rock, Young's modulus and Poisson's ratio might have been changed during overcoring and the biaxial testing. This issue has been studied specifically in this report using FLAC.

The second part of the project, which is presented in this report, is to through numerical modelling in 2D and 3D study how geological discontinuities affect the stress.

2   Geology at Äspö

2.1   Lithology

The lithology for Äspö has been presented in several reports, Stanfors et al (1997), Rhén et al (1997a) and Rhén et al (1997b). Depending on the site scale, the lithological models are different. On the regional scale, the most dominating rock type is Småland granite and on the site scale there are four main rock types, Äspö diorite, Småland granite, greenstone and fine-grained granite.

The Äspö diorite is the most common rock type both on the surface, see Figure 2-1 and in the tunnels. The properties of the different rock types are summarised in Table 2-1.

Table 2-1   Properties of the actual rock types (Stille & Olsson 1996, Stanfors et al 1997).

Rock type	Density (t/m^3)	Young's modulus (GPa)	Poisson's ratio	Uniaxial compression strength (MPa)	RMR
Äspö diorite	2.75	73	0.24	171	69
Småland granite	2.64	74	0.23	255	65
Greenstone	2.96	78	0.24	207	64
Fine-grained granite	2.67	77	0.23	258	48

The following sections describing the rock types are a short summary of a number of reports (Stanfors et al, 1997, Rhén et al, 1997a and Rhén et al, 1997b).

2.1.1   Äspö diorite

The rock is generally grey to reddish grey, medium-grained and contains more or less large crystals of potassium feldspar. The age is well defined to 1804 ± 3 million years. The mineral content of Äspö diorite is quartz 15%, k-feldspar 12%, plagioclase 46% and biotite 15%.

2.1.2   Småland granite

This rock type differs from Äspö diorite because of the brighter, more reddish colour. Two specific differences are the fewer amounts of potassium feldspar and the much more irregularly distributed crystals.

It seems that the Småland granite is a younger formation than the Äspö diorite, since granite intrusions can be seen in the diorite. The difference in age of the two rocks is, however, probably very small.

The mineral content of Småland granite is quartz 25%, k-feldspar 25%, plagioclase 37% and biotite 7%.

2.1.3   Greenstone

Greenstone can visually be distinguished from the granitoid rocks by its very dark, greenish black colour.

The mineral content of Greenstone is amphibole (36%), epidot (9%), plagioclase (27%) and biotite (18%).

2.1.4 Fine-grained granite

The fine-grained granite occurs quite frequently on the island of Äspö, both on the surface and in the tunnel. It appears as dikes and irregular veins and in the whole rock mass, but the number of veins in the Småland granite is sparse compared with the number of veins and dikes in the Äspö diorite. Most of the dikes strike NE.

The mineral content of Fine-grained granites is quartz 30%, k-feldspar 39% and plagioclase 20%.
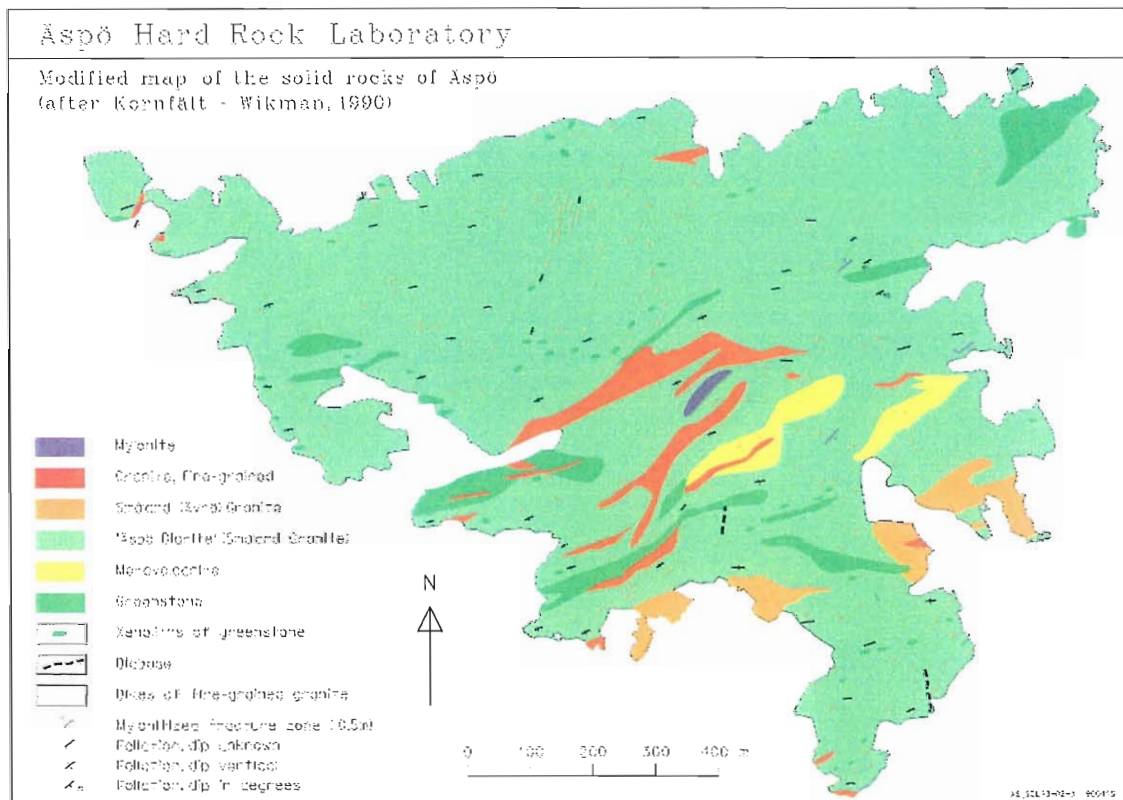
Figure 2-1   *Map of solid rocks at Äspö Island (Rhén et al, 1997b).*

2.2 Geological structures

The SKB geological model is based on surface mapping, drill holes and seismic data at the Äspö island, and consists of several major and minor fracture zones.

The definition of a major fracture zone is that it has a feature more than 5 meters wide and extending several hundreds of meters. A fracture zone between 0.1 and 5 meters wide is defined as a minor fracture zone, Stanfors et al (1997).

The major fracture zones are labelled EW-7, NE-4, NE-3, NE-1, EW-3, NE-2 and EW-1 (Stanfors et al, 1997, Rhén et al, 1997b). The appearance of the structures on the ground surface can be seen in Figure 2-2. Fracture zone EW-5 that was predicted as gently dipping by seismic reflection was not found in the tunnel and does not exist (Stenberg, 2000). The position where the fracture zone intersects the tunnel is measured in the centre of the branch. The orientations of the zones are defined by using strike and dip.

7
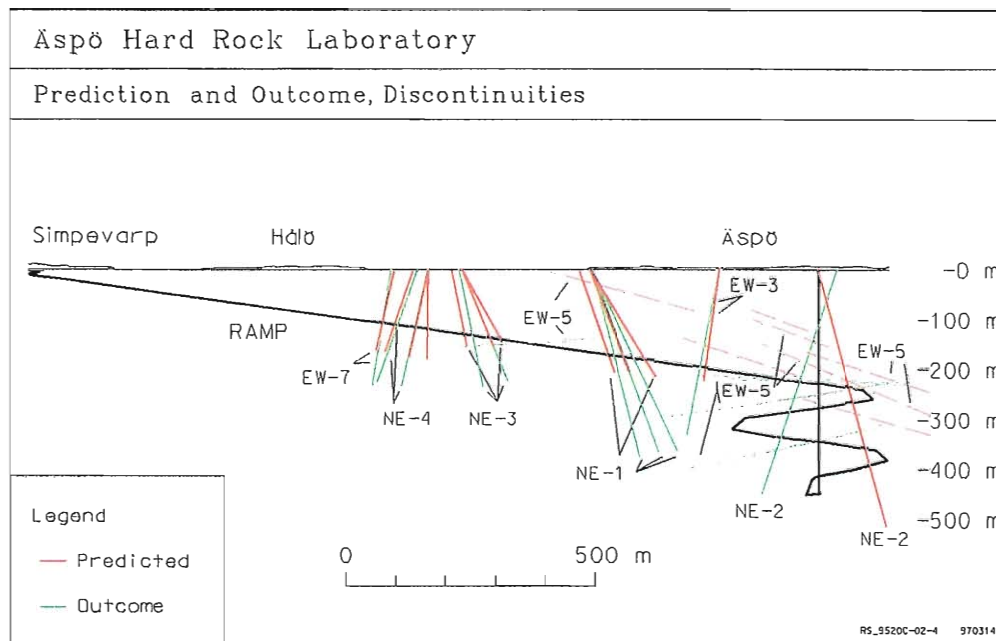
Figure 2-2 *The SKB geological structures (Rhén et al, 1997a).*

2.2.1 Fracture zone EW-7

The zone may be regarded as a composite fracture zone with an orientation of 075/75 (strike/dip). The width of the zones is about 10 metres and contains mainly Småland granite. The fracture zone intersects the tunnel at 787 m and its length is less than 1000 metres.

2.2.2 Fracture zone NE-4

The fracture zone NE-4 consists of two branches with a total width in the tunnel position of 41 metres. The first branch intersects the tunnel at 802 m and has an orientation of 050/60 and the second branch intersects the tunnel at 855 m and has an orientation of 050/43. The dominating rock type in the fracture zone is Småland granite with inclusion of mylonite and greenstone.

2.2.3 Fracture zone NE-3

The fracture zone consists of two sub-parallel branches with a total width in the tunnel position of about 49 metres. The first branch with an orientation of 310/80 intersects the tunnel at 975 m and the second branch with an orientation of 290/70 intersects the tunnel at 1009 metres. Both branches have a length of more than 1000 metres. The dominating rock type of the fracture zone is fine-grained granite, with some intersections of Småland granite and greenstone. Its constituent fractures are steep and strike EW and NS. Their fracture surfaces are coated mainly with chlorite and calcite, but also with clay, fluorite, hematite and iron oxide.

2.2.4 Fracture zone NE-1

The fracture zone consists of three branches with a total width of 61 metres. The first branch has a width of 25 metres and intersects the tunnel at 1263 m. The orientation of the branch is 310/75. The second branch, which has a width of 8 metres and an orientation of 310/75, intersects tunnel at 1280 metres. The first and second branches are very close to each other. The third branch has an orientation of 300/70 and a width of 28 metres and intersects the tunnel at 1305 metres. All of the branches have a length

8

of more than 500 metres. The branches intersect a rather complex rock mass with Äspö diorite, fine-grained granite and greenstone. The fractures within the zone do not differ from the fractures in the average rock mass in any sense, except for a slight increase in epidotic/quartzitic coatings and minor mylonite shear zones.

2.2.5   Fracture zone EW-3

EW-3 is estimated to be about 14 m wide and has an orientation of 080/75. The fracture zone, which consists of a 2-3 m wide crushed zone connected to the contact between Äspö diorite and fine-grained granite, intersects the tunnel at 1414 m. The crushed zone is surrounded by 5-10 m of highly fractured Äspö diorite. In the crushed zone clay altered rock is common. The length of the fracture zone is less than 1000 meters.

2.2.6   Fracture zone NE-2

The fracture zone intersects the tunnel at three different levels. The first position in the tunnel is at 1602 metres where the orientation of the zone is 036/82 and the width of the zone is 1 meter. The second intersection in the tunnel is at 1844 m with an orientation of 015/70 and a width of 1 meter. The zone intersects the tunnel finally at 2480 m with an orientation of 032/65 and a width of 5 meters.

2.2.7   Fracture zone EW-1

This fracture zone is a part of the 300 meters wide low-magnetic zone. The zone can be regarded as the northern part of the Äspö shear zone. The zone strikes NE and divides Äspö into two main blocks. EW-1 consists of at least two branches, with an orientation of 045/78 and 045/88, Rhén, et al (1997b). The fracture zones do not intersect the tunnel.

9

3 Numerical modelling of overcoring and biaxial testing

The results the first part of this research "Rock Stress and Rock Stress Measurements at Äspö HRL" showed that the magnitudes of the rock stresses obtained by the overcoring technique were higher than those determined by the hydraulic fracturing technique (Lundholm, 2000). One explanation to this discrepancy is high values of the Poisson's ratio. A study of the behaviour of the rock core during overcoring and biaxial testing was therefore initiated. The main question is whether boreholes drilled perpendicularly or parallel to the major principal stress will result in extensional strain, which may initiate and propagate fractures.

The study by Martin and Christiansson (1991) showed that the greatest number of microcracks were created in overcored samples from boreholes oriented approximately perpendicular to the direction of the major principal stress. They found that the presence of the stress-induced microcracks resulted in anisotropy of the mechanical properties in grey and pink granite cores. The cores containing a higher number of microcracks showed a higher value of Poisson's ratio. The phenomenon with stress-induced could be closely-related to core discing. Durelli et al (1968) and Stacey (1982) among others presented that the mechanism behind core discing occurs as a result of high stresses perpendicular to the core.

This raised the question if microcracking also occurred in the rock cores in the vertical borehole KA3579G since extremely high vertical stresses were obtained in the overcoring stress measurements (Ljunggren and Bergsten, 1998). The measurements in this borehole that resulted in high vertical stresses were conducted 2-4 meters below the floor of the tunnel. Larger magnitudes than expected were also obtained at larger depth. The borehole is drilled from the tunnel floor, which is about 485 meters below the ground surface.

The biaxial tests showed that the cores taken from the horizontal borehole, KA1899, which is drilled in the direction of the major principal stress at Äspö, had high Poisson's ratios (Lee et al, 1994). For instance, one core samples from KA1899 has a Poisson's ratio of 0.41. The rock stress measurements at this location resulted in a major principal stress of 21.3 MPa with a orientation that is almost parallel with the borehole axis and the intermediate and minor principal stresses of 7.9 MPa and 6.6 MPa, respectively (Lee at al, 1994). These stresses have been used in the numerical model simulating overcoring and biaxial testing. Since the Poisson's ratio at this measurement point is quite high, this may have an influence on the achieved stresses.

3.1.1 Background

For a homogeneous, isotropic, linear elastic material the stresses in the material are determined through the change of the strains during the overcoring. The elastic properties, Young's modulus, E and Poisson's ratio, v are obtained from a biaxial test of the hollow core (σ_3 is equal to zero and parallel to the borehole axis). The minor principal strain is expressed as

$$\varepsilon_3 = \frac{1}{E}[\sigma_3 - v(\sigma_1 + \sigma_2)] \tag{3-1}$$

according to Hooke's law. The minor principal strain on the inner wall of the core during biaxial testing will be parallel to the core axis (ε_z) and perpendicular to the wall of the pilot hole (ε_r). It is seen in Equation 5-1 that ε_3 may become negative, i.e. extensional, when $\nu(\sigma_1 + \sigma_2) > \sigma_3$.

Stacey (1981) presented a failure criterion that states that fracture of brittle rock will initiate when the total extension strain in the rock exceeds a critical value, ε_c, which is characteristic of the rock type. This means that fractures may be initiated and propagated in the core when it is exposed to the critical extension strain. The assumption of the linear elastic behaviour for the rock material is in such a case violated. Considering this phenomenon in the overcoring technique, a few cases can be highlighted and the consequences described.

In the first case, no microcracks are induced during the overcoring. The core is then pressurised in a biaxial cell, which may induce microcracks. These microcracks could influence the Poisson's ratio that is evaluated from the biaxial testing. The strains that are measured during the overcoring are unaffected by microcracks, but due to the high Poisson's ratio the stress parallel to the borehole is higher than the true stress in the rock mass. This problem will be investigated in more detail in FLAC by simulating the biaxial testing of a fresh virgin core.

In the second case, the overcoring induced microcracks in the core. This may occur when the major principal stress is perpendicular to the borehole axis. The consequence of this may be that large stresses are obtained from the evaluation of the stress measurements along the borehole. The induced microcracks from the overcoring can affect the Poisson's ratio that is achieved from the biaxial testing since opening and/or sliding of the microcracks may occur during the biaxial testing of the core. However, how much the Poisson's ratio is affected depends probably on the orientation of the microcracks. If the microcracks are orientated crosswise, see Figure 3-1, they probably affect the Poisson's ratio more since the biaxial pressure squeezes the middle part of the core and the movement occurs along the microcracks i.e. sliding occurs. The orientations of the microcracks are highly dependent on the orientation of the principal stresses.
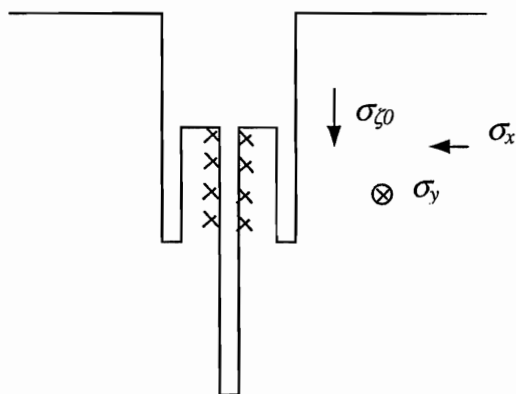
Figure 3-1   *A schematic sketch of the stresses during overcoring.*

The stresses will always be parallel and perpendicular to the borehole boundary, assuming that the boundaries are not loaded by the strain gauges in the pilot hole, regardless the *in situ* stress state. However, the stresses caused by the drillbit can yield in shear stress at the borehole boundary. Considering these circumstances, if σ_{z0}, σ_x and σ_y are principal stresses the microcracks should mainly be oriented parallel and perpendicular to the borehole, while if σ_{z0}, σ_x and σ_y are not principal stresses, the minor strain can occur in any orientation. The microcracks could then be initiated in orientations other than parallel and perpendicular to the borehole. The Poisson's ratio estimated in these cases is not correct since the assumptions of linear elasticity have been violated.

3.2   FLAC modelling of overcoring

To study the behaviour of the core during overcoring an axisymmetric *FLAC* model has been used since it provides an analysis of the boreholes stresses closely related to the three dimensional conditions (Itasca, 1998a).

The modelling is divided into two separate analyses. In the first analysis, overcoring is simulated to investigate the re-distribution of the stresses and strains in the core at different stages of the drilling. The drilling process is divided into two stages: drilling of the pilot hole and overcoring of the sample. In the second analysis, a biaxial test of the tube core is simulated. The stresses induced by the drillbits are not taken into consideration.

Two principal different stress situations were analysed (Figure 3-2):

−   The far-field major principal stress is parallel to the borehole axis

−   The far-field major principal stress is perpendicular to the borehole axis

These analyses were made using the same model with rock properties as can be seen in Table 3-1. The strain gauges were assumed to be installed in the middle of the hollow core. During the analyses, drilling of the pilot hole and the overcoring were simulated in four steps.

1.   The first half of the pilot hole was drilled

2.   The second half of the pilot hole was drilled

3.   The first half of the overcoring was performed

4.   The second half of the overcoring was made.
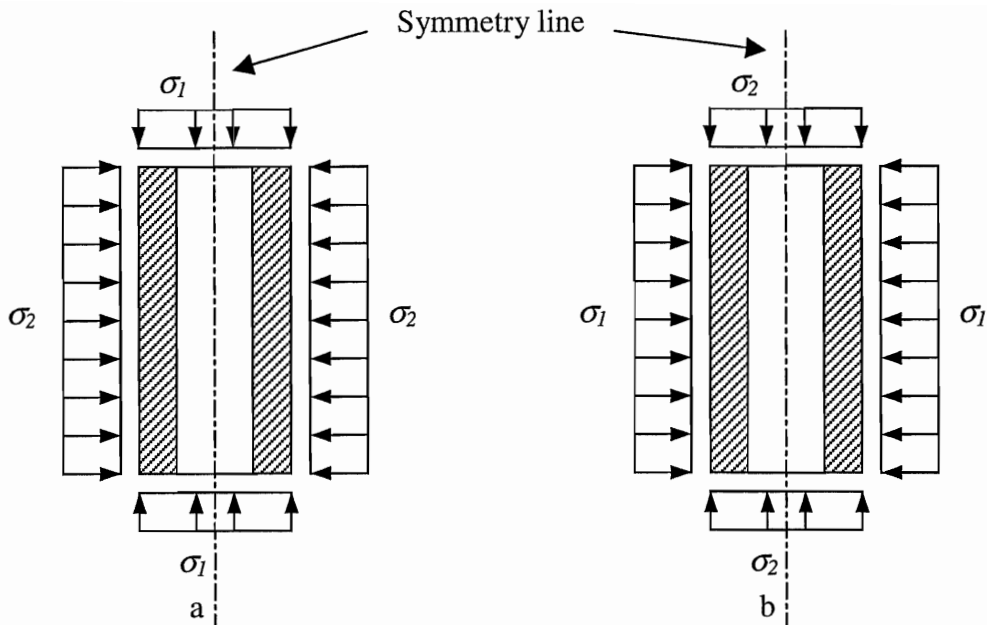
Figure 3-2 *Illustration of the two axisymmetric FLAC models. Major principal stress parallel to borehole axis (a) and major principal stress perpendicular to the borehole axis (b).*

3.2.1 Boundary condition

Two boundaries of the model, the left and the bottom have zero normal displacement. The stresses were applied on the right and the upper boundaries, which is illustrated in Figure 3-3. The loading condition in this axisymmetric model is similar to that in a biaxial test, except that an axial stress is also applied. The left boundary is the symmetry axis and the centre line of the borehole, which is shown in the close-up of the model in (Figure 3-4). The radius of the pilot hole was 19 mm and the radius of the large hole was 38 mm. The radius of the overcored core was 36 mm. This model was used for analysis F1, F2, F3 and F4 (Table 3-1).

13
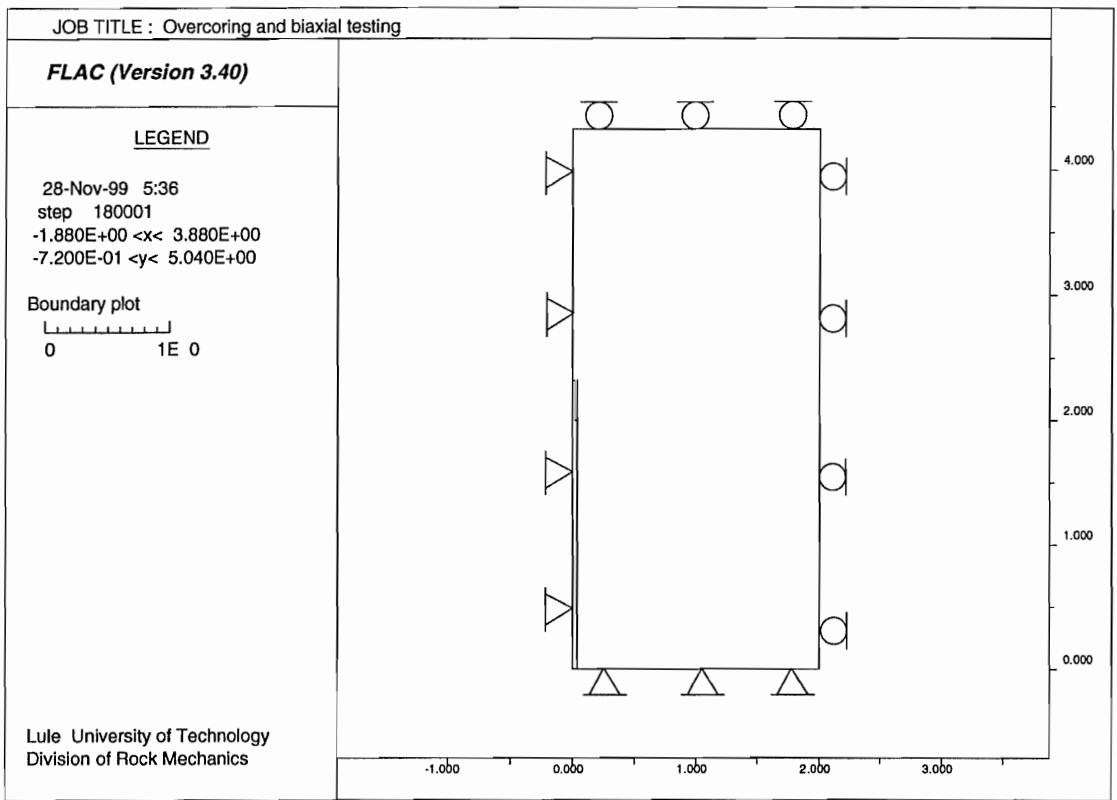
Figure 3-3   *FLAC model of overcoring.*
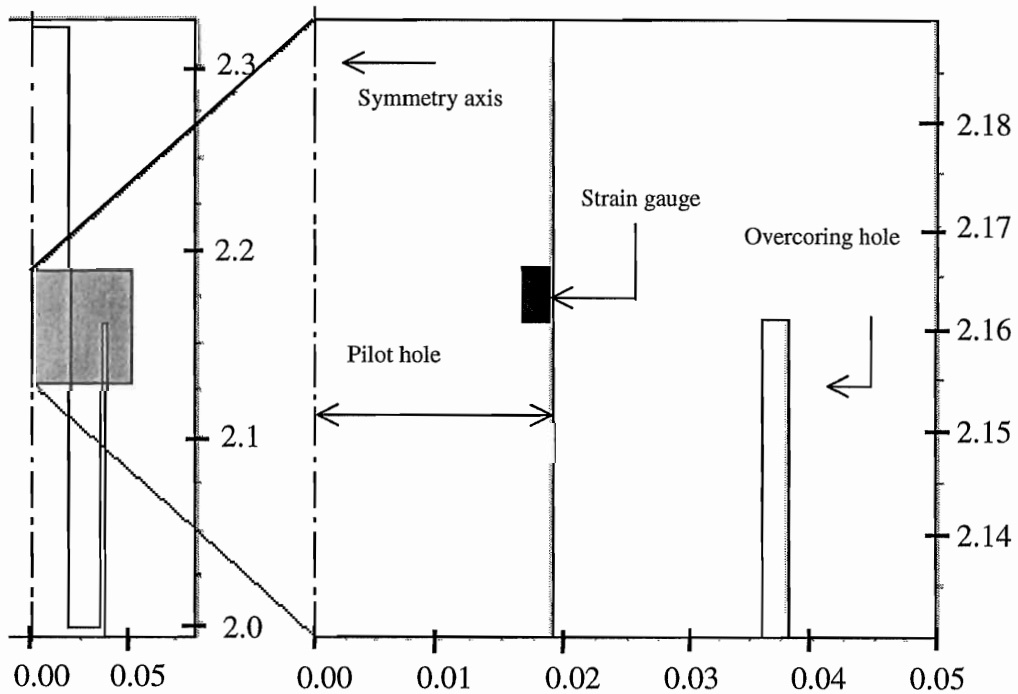
Figure 3-4   *A detailed schedule of the overcoring model.*

14

The stresses measured at point #1 in the horizontal borehole KA1899A (Lee et al., 1994) are applied to the first two analyses F1 and F2. The major principal stress, 21.3 MPa is applied parallel to the core. The stress that is applied perpendicular to the axis of the core is the mean value of the intermediate and minor principal stresses and equal to 7.3 MPa.

The other two analyses F3 and F4 represent the vertical borehole KA3579G at Äspö. The borehole was drilled from the floor of the TBM excavated tunnel at 480 metres below ground surface. To achieve a fair estimation of the stress distribution around the tunnel a numerical simulation by $Examine^{3D}$ has been made. The diameter of the tunnel is 5 metres and the virgin stresses used in the $Examine^{3D}$ model are given by Equations 4-3 and 4-4. Average values of the vertical and the horizontal stresses over a length of 2 metres of the borehole just below the tunnel floor (Figure 3-5) were used as axial and radial stress, respectively, in the analyses of F3 and F4. The input data for all the four analyses F1 to F4 are presented in Table 3-1. The cohesion and the friction angle were determined from the relation that the tensile strength is 10% of the compressive strength of the intact rock. The elastic model was used to calculate the strains and the Mohr-Coulomb plasticity model has been used in order to study the non-elastic behaviour of the rock.
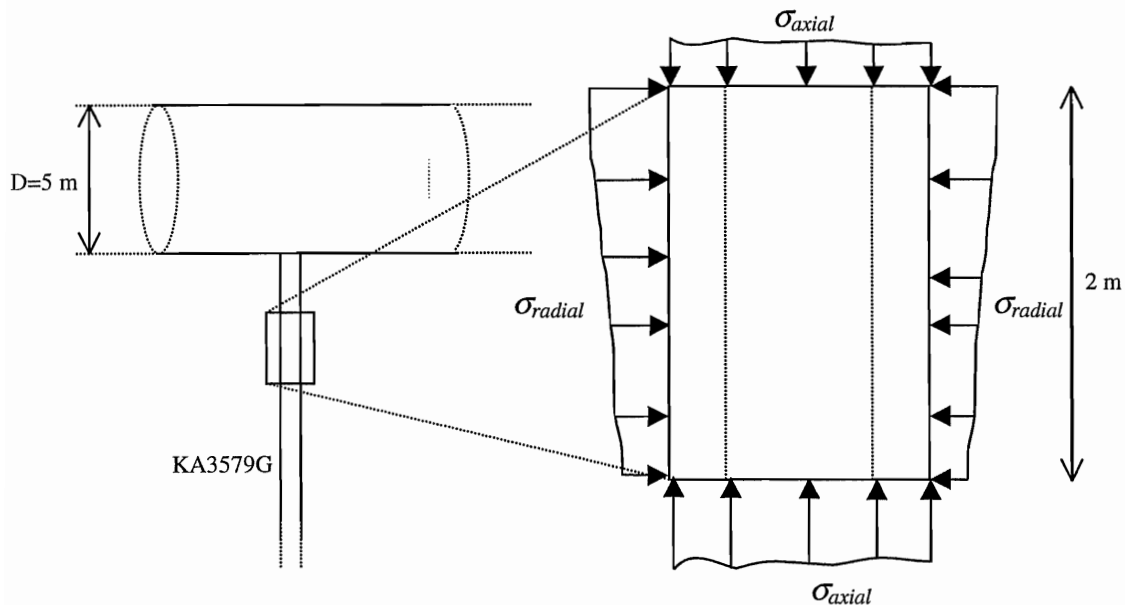
Figure 3-5.   *A schematic figure over the Examine 3D model.*

Table 3-1   **Values of the parameters used in the four numerical models.**

Model	F1	F2	F3	F4
	σ_1 parallel to borehole		σ_1 perpendicular to borehole	
σ_1 [MPa]	21.7	21.7	25	25
σ_2 [MPa]	7.3	7.3	10	10
ν	0.24	0.24	0.24	0.24
E [GPa]	73	73	73	73
c [MPa]	2.7	2.7	2.7	2.7
ϕ [°]	55	55	55	55
σ_t [MPa]	1.7	1.7	1.7	1.7
Type of model	M-C plasticity	Elastic	M-C plasticity	Elastic

3.2.2 Results

The simulation of the pilot hole shows that hardly any damage occurs in the core. Therefore, attention will only be paid to the overcoring process. The presentation of the results have been focused to the stage of the overcoring when the overcoring drill bit is at the same axial position as the strain gauges, see Figure 3-6.

The results from the two different types of stress situations (σ_l // with the borehole and $\perp$ to the borehole) during overcoring is presented together in Figure 3-6 in order to compare these two cases.

When the far-field major principal stress is parallel to the borehole axis the minimum principal stress in the area of the strain gauges is about -5 MPa i.e. compressive (Figure 3-6a). On the other hand, when the far-field major principal stress is perpendicular to the borehole axis, the secondary minor principal stress at the position of the strain gauges is 10 MPa i.e. tensile (Figure 3-6b).
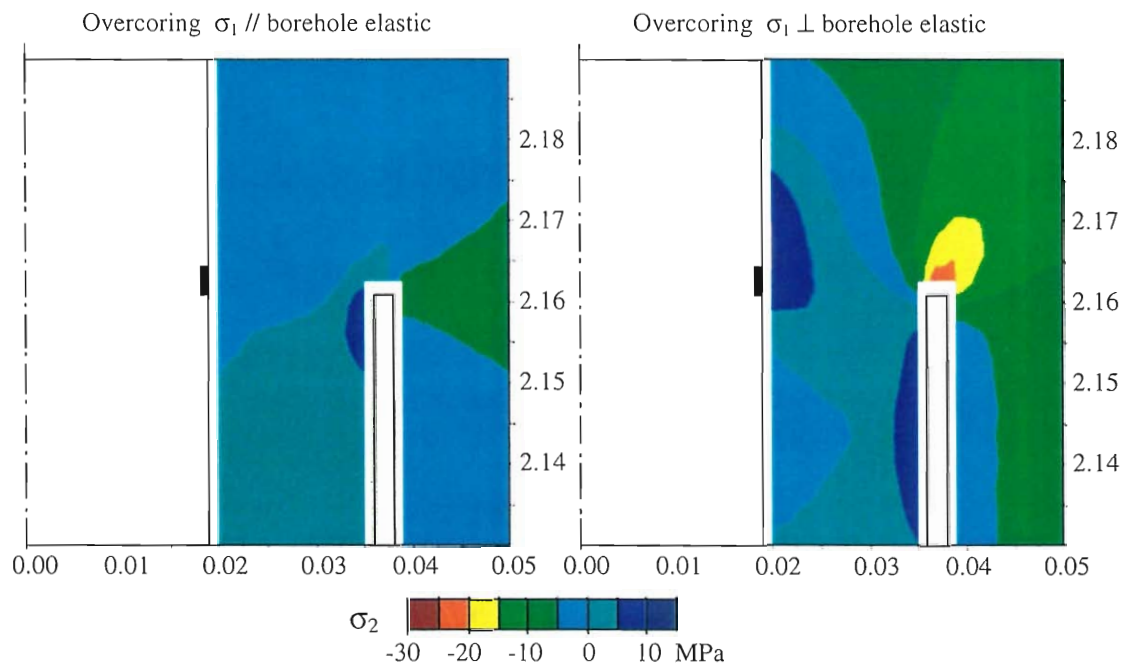
Figure 3-6   *The contours of the minimum stress contours during overcoring (tension = "positive" value).*

Comparing the two different far field stress situations considering the strains in the core, extensional strains may occur in both cases, see Figure 3-7. However, the extensional strain is higher in the case where the far-field major principal stress is applied perpendicular to the borehole than parallel. In the former stress situation, extensional strains up to 300 microstrains is achieved, whereas only 100 microstrains in the latter stress situation. Mohr-Coulomb criterion/model, however, can not predict failure due to large extensional strains. From the plastic analysis, the yielded zones can be visualised, indicating a slightly larger yielding area when the major principal stress is applied perpendicular to the borehole, see Figure 3-8. However, the analyses do not indicate if it is a pure tensile or shear failure or a combination of these two failure mechanisms.
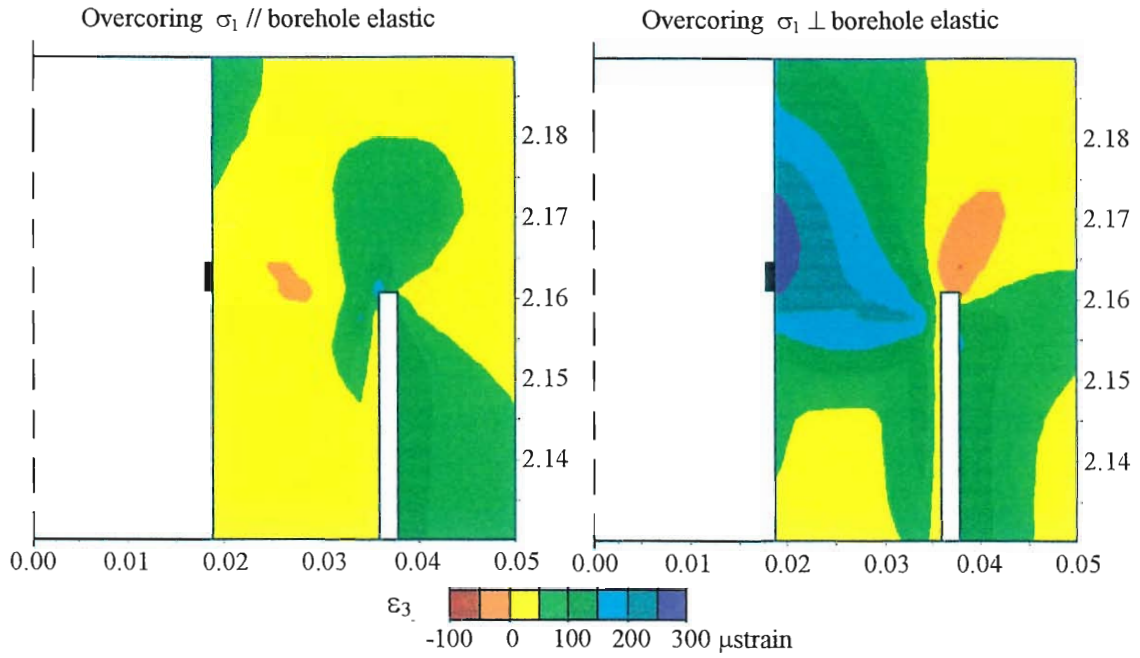
Figure 3-7 *The contours of the minimum strain contours during overcoring (tension = "positive" value).*
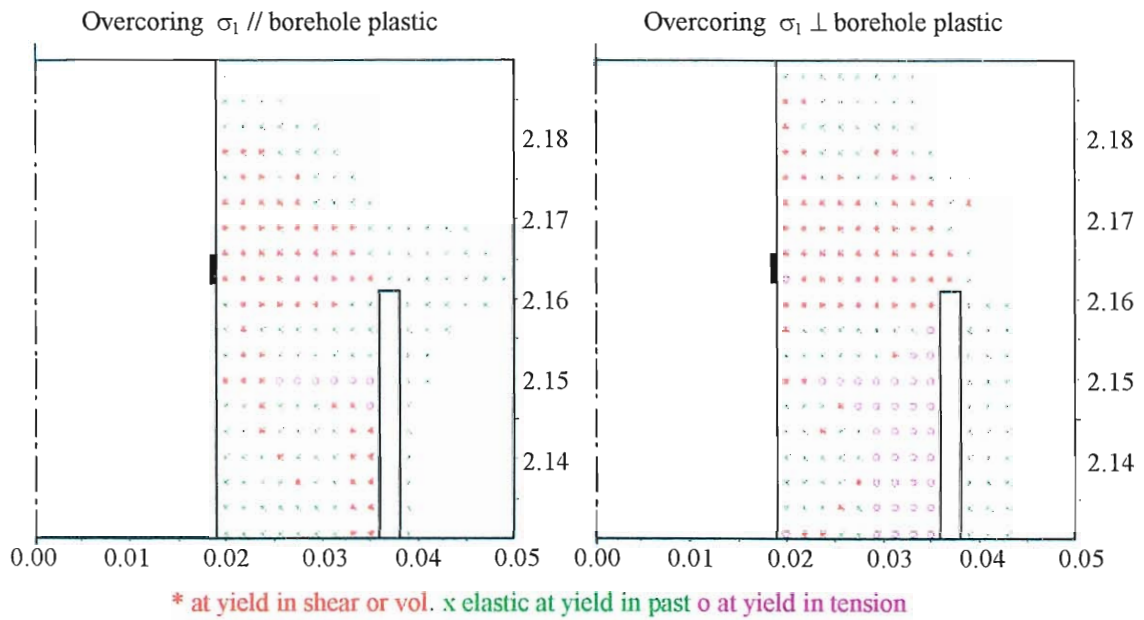
Figure 3-8 *Plastic zones during overcoring.*

3.3   FLAC modelling of biaxial testing

 The biaxial testing of a core is simulated using a *FLAC* model. Two kinds of core samples, a core damaged during overcoring and a fresh intact core are investigated. In the first case, the core exposed to overcoring from Model F1 is used. In the second case an undamaged virgin core was used. The same material properties are used for the biaxial models as in the overcoring models, see Table 3-1. During the biaxial testing a radial pressure of 20 MPa was applied at the middle section of the core over a length of 200 mm, see Figure 3-9. The radial pressure was achieved by applying a velocity boundary over these 200 mm. The model was then cycled until the pressure on the core reached 20 MPa.
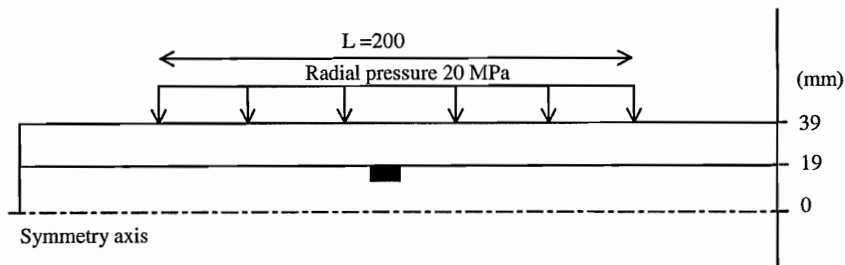
Figure 3-9.   *FLAC model of the biaxial testing.*

3.3.1   Results

Figure 3-10 shows the minimum principal stress and strain in a virgin core. The extensional strain is more than 175 microstrains at the inner boundary of the virgin core and the minimum principal stress is about 0.15 MPa (compression). Figure 3-11 is a comparison of the yield zones in the fresh core and in the core damaged by overcoring. It is seen that yielding occurs in the whole core damaged by overcoring, while only partly in the fresh core.
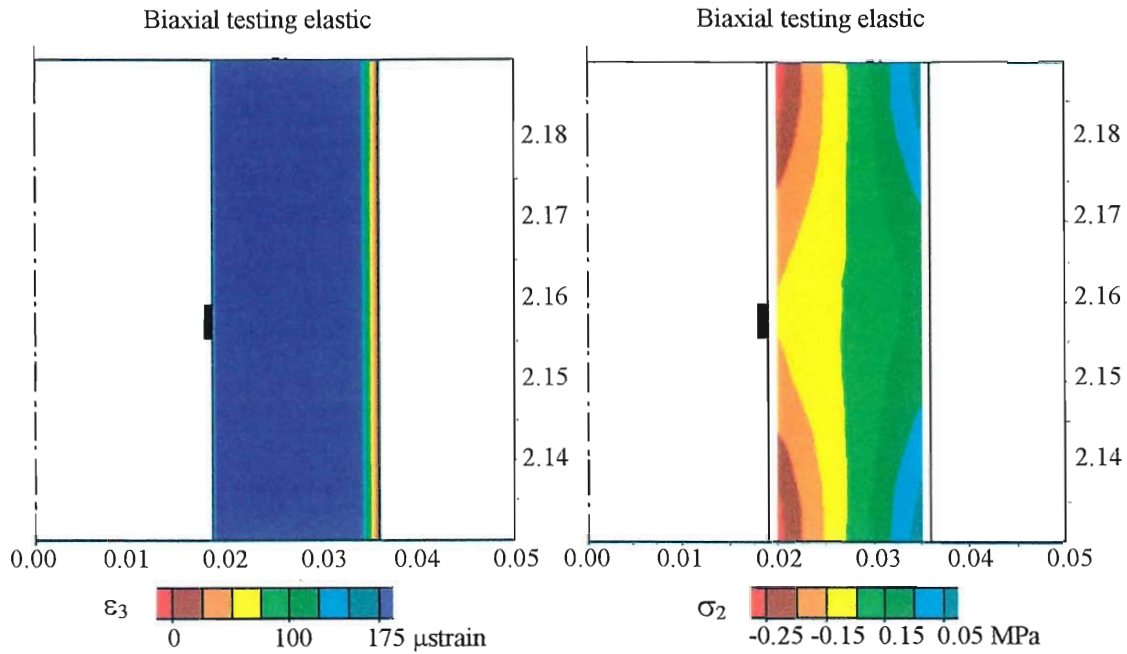
Figure 3-10   *Minimum strain (left) and stress (right) contours during biaxial testing of a fresh core.*
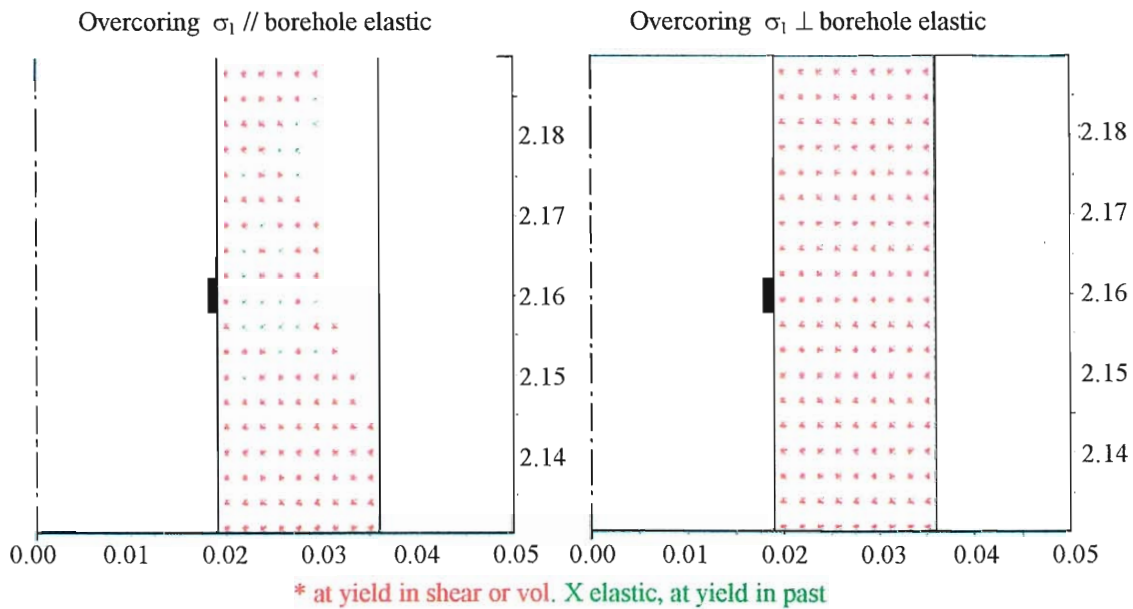
Figure 3-11   *Plastic zones during biaxial testing of a fresh core (left) and an overcoring core (right).*

3.4   Discussion

Originally, the stresses are acting in all orientations on the borehole where the rock stress measurements are conducted. The core is then removed from the borehole and consequently unloaded. During the biaxial test the core is exposed to a radial pressure but no axial pressure. Considering this, the strains of the core are measured when the principal stresses acting on the core are non zero, while the elastic properties of the rock, are determined when no confining pressure is acting perpendicular to the axis of the core. The core is still unloaded in one direction. Whether this discrepancy in the

19

stress state creates significant errors in stress estimations needs to be further investigated.

3.4.1 Overcoring

When the major principal stress is applied perpendicular to the borehole, the extensional strain ($\varepsilon_3 = 300$ µstrain) is larger on the inner surface of the core during overcoring than when parallel to the borehole ($\varepsilon_3 = 100$ µstrain). An extensional strain of 300 microstrains may have resulted in microcracking in the core since the critical extensional strain for microcracking in rock types similar to those present at Äspö has been reported to be about 250 *µstrain* (Stacey, 1986).

3.4.2 Biaxial testing

It can be seen from the simulation of the biaxial testing that even an intact core can be exposed to quite large extensional strains. This means that even if cautious drilling does not create damage to the core, the core can still be damaged during biaxial testing, which will cause errors in the estimated values of the elastic properties.
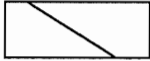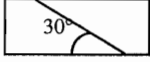
3.5 Conclusion

When microcracks are initiated and propagated in the core during overcoring, the estimated stresses may deviate from their true values since the measured strains also include opening of small cracks. On the other hand, if the microcracks are opened or propagated during the biaxial test, this may result in a high Poisson's ratio and then introduce error in the transformation from strains to stresses.

4 Numerical modelling of a single discontinuity

In order to improve the understanding of how and to what extent discontinuities affect the state of stress, several analyses using conceptual models have been performed using UDEC (Itasca, 1996). The models used in each analysis are presented in Table 4-1.

Table 4-1. Models to analyse a single discontinuity.

Model	Analysis	Variable parameters	Model outline
1	Discontinuity with varying dip angle.	Dip angle	
2	A 50 metre thick zone with high strength contacts.	Young's modulus & Poisson's ratio of the zone material	
3	Stiffness related to the mechanical width of a zone.	Normal and shear stiffness of the discontinuity	
4	A 50 metre thick zone with low strength contacts.	A combination of model 2 and 3.	

In the first model the effect of the dip angle of a single discontinuity is studied. The second model was used to study the effect of the stiffness of the rock material in a zone. High strength contacts were used to isolate the study to the elastic properties of the zone. The second approach to study the effect of a zone of different mechanical properties was made in the third model. In this model the thickness of the zone, here defined as the mechanical width of the zone was replaced by a single discontinuity with normal and shear stiffness based on the width of the zone (Hakami et al, 1998). The fourth model is a combination of model 2 and 3 in order to study the effect of a 50 metre wide zone with low strength contacts.

The model is 6000 m wide and 3000 m high and fictitious joints are used to divide the model into areas with different zone size. The strength and stiffness parameters was given extremely high values in order to prevent non-elastic deformations and therefore minimise the disturbance of the fictitious joints on the state of stress.

Table 4-2. Mechanical properties used in all the models.

Mechanical Parameters	Value
Density	2750 kg/m^3
Young's modulus	73 GPa
Poisson's ratio	0.24

The far field stresses used in the models are the virgin state of stress in Fennoscandia (Stephansson et al., 1991),

$$\sigma_H = 2.8 + 0.04z \qquad \text{(MPa)} \qquad\qquad 4\text{-}1$$

$$\sigma_h = 2.2 + 0.024z \qquad \text{(MPa)} \qquad\qquad 4\text{-}2$$

The upper boundary is the ground surface. At the other three boundaries stress boundary conditions are applied. The major horizontal stress is acting in the plane.

In order to examine the effect of the discontinuity, the stresses are normalised with respect to a homogenous model without any discontinuities or zones. At each depth, the major principal stress in the model with a discontinuity is divided by the major principal stress in a model without a discontinuity. This results in a factor,

$$R_1 = \frac{\sigma_1{}^i}{\sigma_1{}^0}$$

4-3

where $\sigma_1{}^i$ is the major principal stress along the fictitious line in the model with a discontinuity and $\sigma_1{}^0$ is the major principal stress in any model without a discontinuity. The same is done for the minor principal stress, the vertical stress and the horizontal stress. These ratios are denoted R_2, R_v and R_h. By presenting the stress ratios instead of the stresses versus the depth below the ground surface, comparison between different kinds of models can be done without jeopardise that the results is also affected not only by the tested parameters but also by the model itself.

Since the principal stresses in the model without a discontinuity were determined, a check was made that no influence from the boundaries occurred and a homogeneous stress state was obtained

4.1 The effect of dip angle

4.1.1 The model

This model contains of one real joint with dip angle α, see Figure 4-1. Five different dip angles of the real joint $\alpha = 0°$, 30°, 45°, 60° and 90° were analysed.
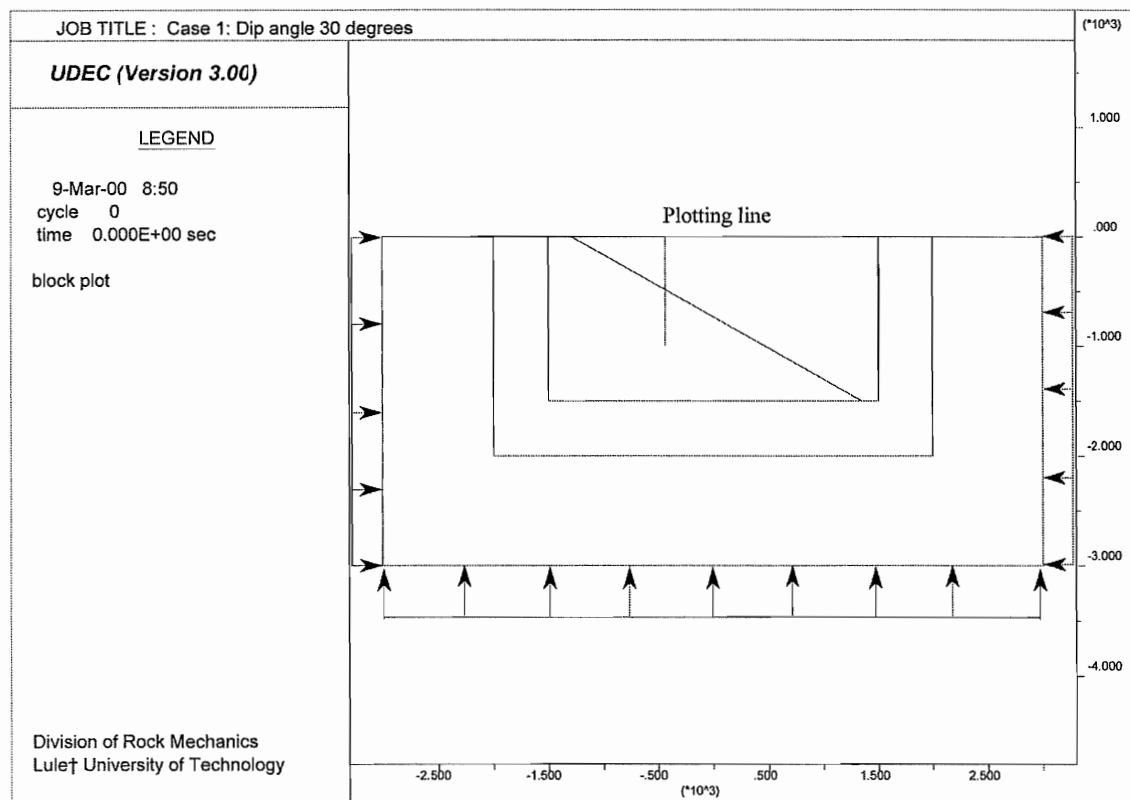
Figure 4-1. *The dip angle model*

The discontinuity properties used in the model are summarised in Table 4-3. In order to determine the effects of the friction angle on the behaviour of the discontinuity both 10 degrees and 20 degrees was used for a discontinuity with a dip angle of 30 degrees. Since almost no stress changes occur in the model with dip angle 30 degrees when the friction angle is 20° (Figure 4-2), a friction angle of 10 degrees is used in the rest of this study, otherwise almost elastic conditions are obtained. A simple equilibrium model can also explain this in which updip sliding occur when

$$\frac{\sigma_h}{\sigma_v} \geq \frac{\tan(\alpha + \phi)}{\tan \alpha} \tag{4-4}$$

where α is the dip angle of the discontinuity and ϕ is the friction angle of the same. This gives that no sliding occurs when the stress ratio, σ_h/σ_v is less than 2 and the friction angle is equal or larger than 20 degrees for any dip angle. In the UDEC analyses the stress ratio of 2.0 or less appears 200 m below ground surface and deeper. However, this reflection does not consider if sliding occur at one location along the discontinuity which causes stress distribution which then causes sliding at a new location along the discontinuity. The cohesion and tensile strength are set to zero in all cases.

Table 4-3. The properties of the discontinuity used in the model.

Mechanical Parameters	Value
Joint normal stiffness	$1 \cdot 10^{11}$ Pa
Joint shear stiffness	$1 \cdot 10^{11}$ Pa
Joint friction	10°
Joint cohesion	0 Pa
Joint tension	0 Pa
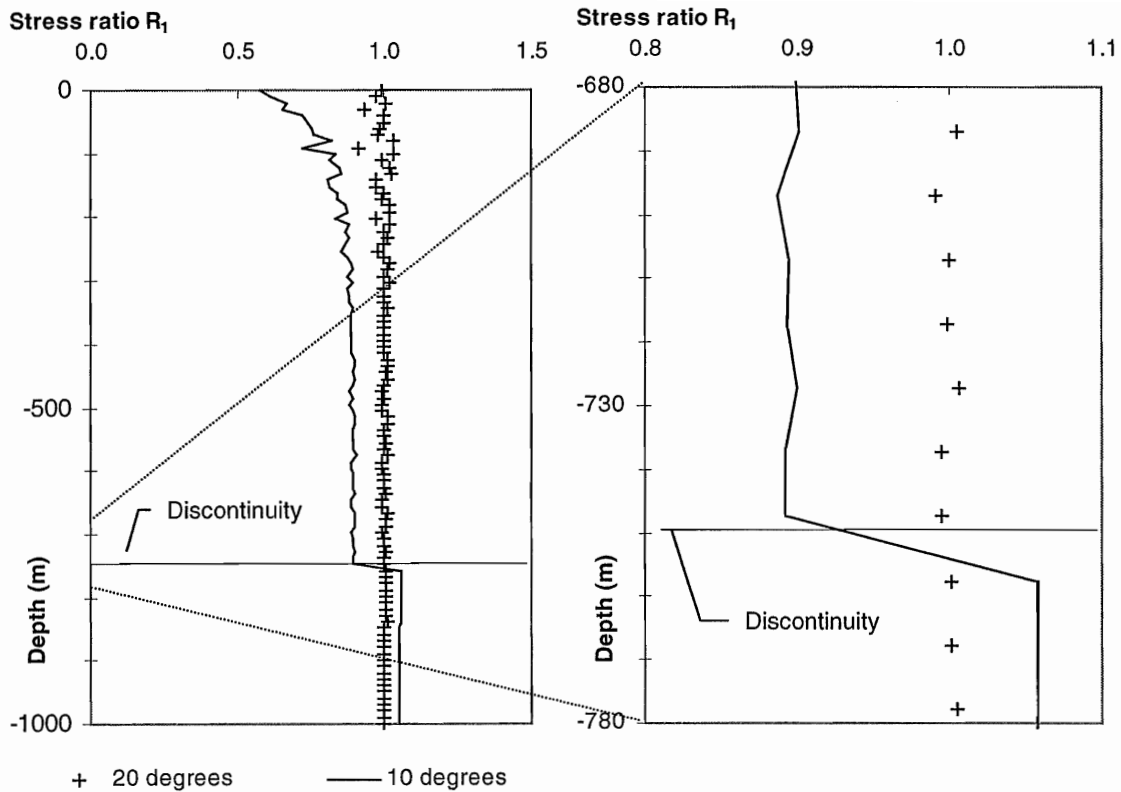
Figure 4-2. *The effect of different friction angles on the stress ratio, R_1*

4.1.2 Results

An inclined discontinuity significantly changes the magnitudes of the major principal stress close to and especially above the discontinuity. In the case of a horizontal discontinuity the stresses are not affected since the stresses are applied parallel and perpendicular to the discontinuity. Figure 4-3 shows the stress ratio, R_1 and R_2. Some of the variation is due to the fact that the zones are not infinitesimal in the numerical model. The figures are zoomed in Figure 4-4 to illustrate the stress changes near the discontinuity.

The variation in orientation of the major principal stress is shown in Figure 4-6. The variation of the stress trajectories near the discontinuity is plotted in Figure 4-7. The orientation is measured clockwise from the y-axis, meaning that an orientation of 90 degrees represents a horizontal orientation. In Table 4-4 the results from the analyses are summarised in numbers.

Table 4-4. Summary of the results.

Dip angle (°)	Stress ratio, R_1			Stress ratio, R_2			Orientation of $\sigma 1$ (°)		
	Before	**After**	**Diff.**	**Before**	**After**	**Diff.**	**Before**	**After**	**Diff.**
0	1.0	1.0	0.0	1.0	1.0	0	89.5	89.5	0.01
30	0.86	1.06	0.19	1.02	1.11	0.09	99.5	79.7	19.7
45	0.91	1.01	0.10	0.96	1.18	0.22	104.4	82.3	22.1
60	0.99	1.01	0.02	0.95	1.08	0.13	94.7	87.7	7
90	1.0	1.0	0.0	1.0	1.0	0	90.3	89.7	0.7

24
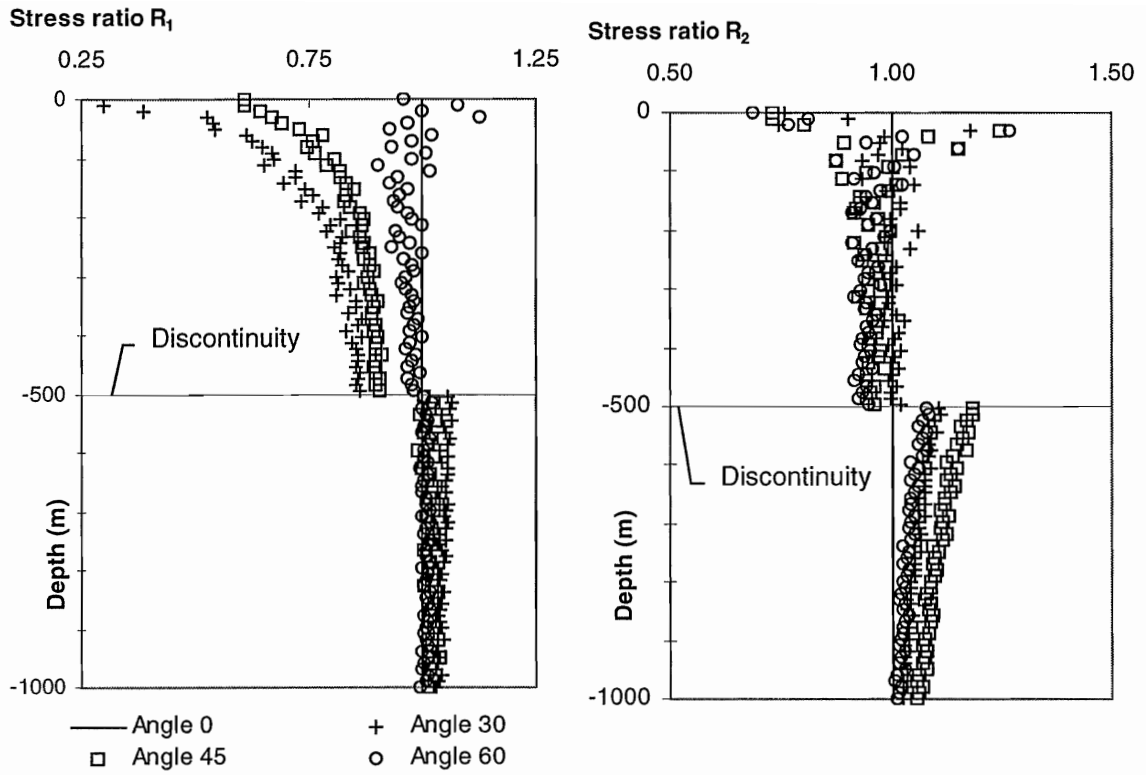
Figure 4-3. *The effect of the dip angle on the stress ratios.*
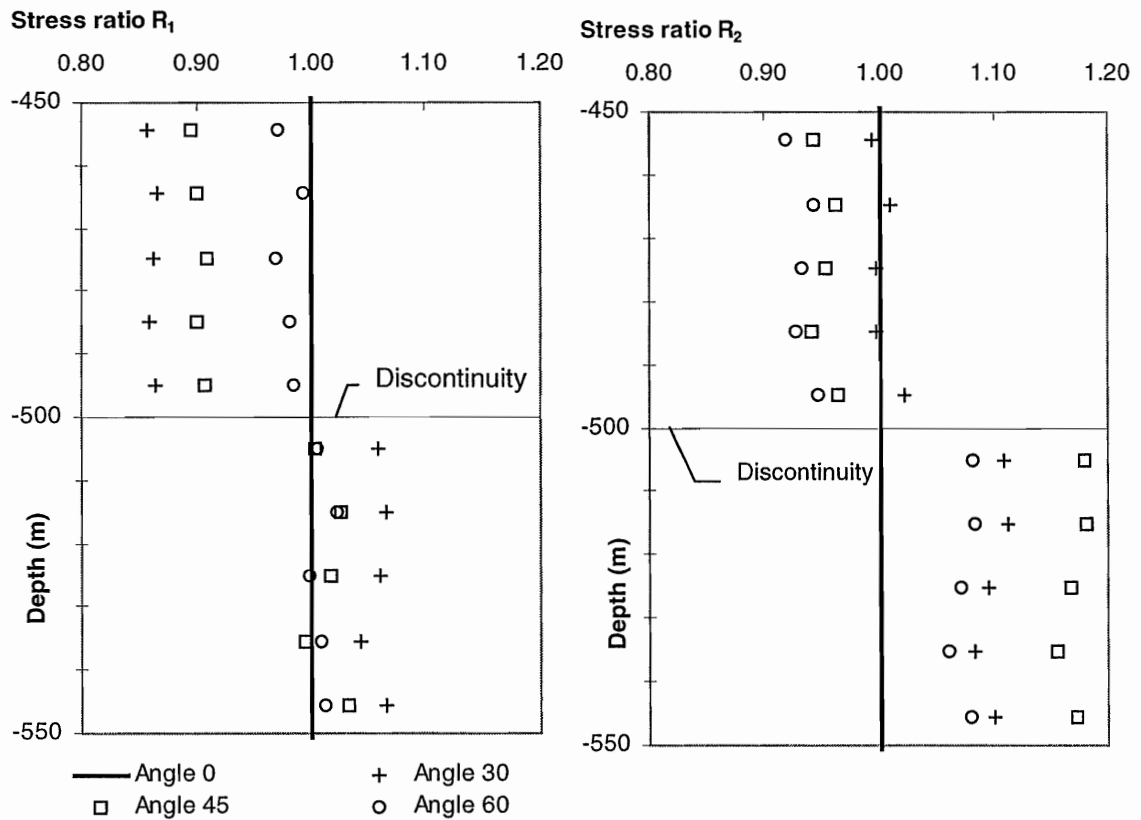
Figure 4-4. *The effect of dip angle on the stress ratios (depth interval from -450 to -550 m).*

The decrease in the stress ratios in the models with a dip angle of 30 and 45 degrees depends on the unloading in the horizontal direction of the upper block. This is because block A is sliding along the discontinuity, which result in a stress release at the left apex of the block A, see Figure 4-5.
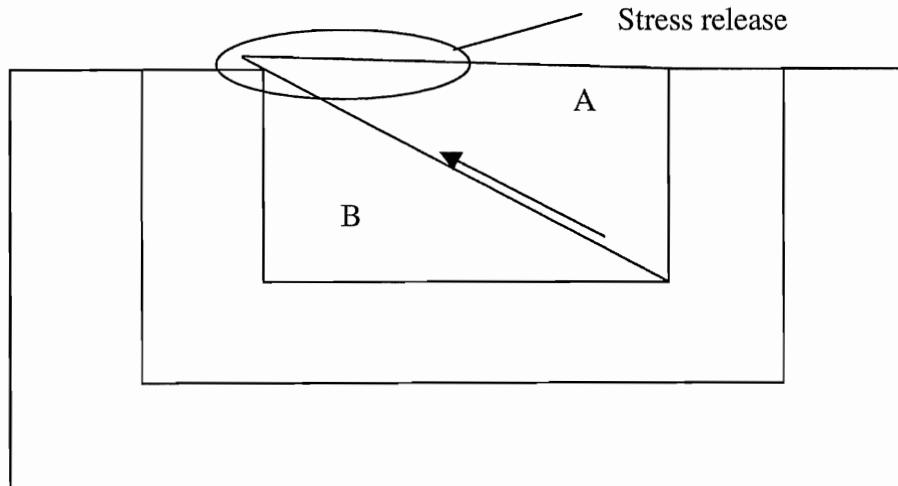
Figure 4-5. *Magnified schedule of the movements of the block.*
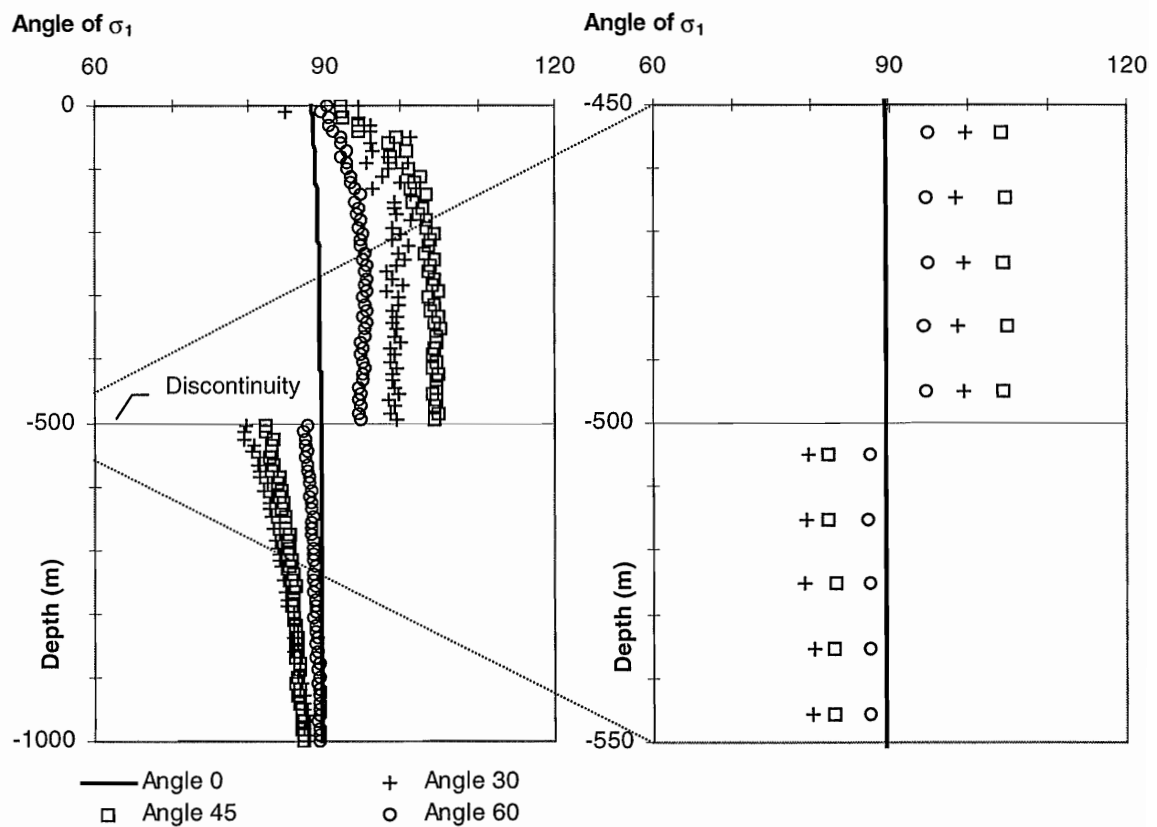
Figure 4-6. *The variations of the orientation of the major principal stress due to different dip angles of the discontinuities.*
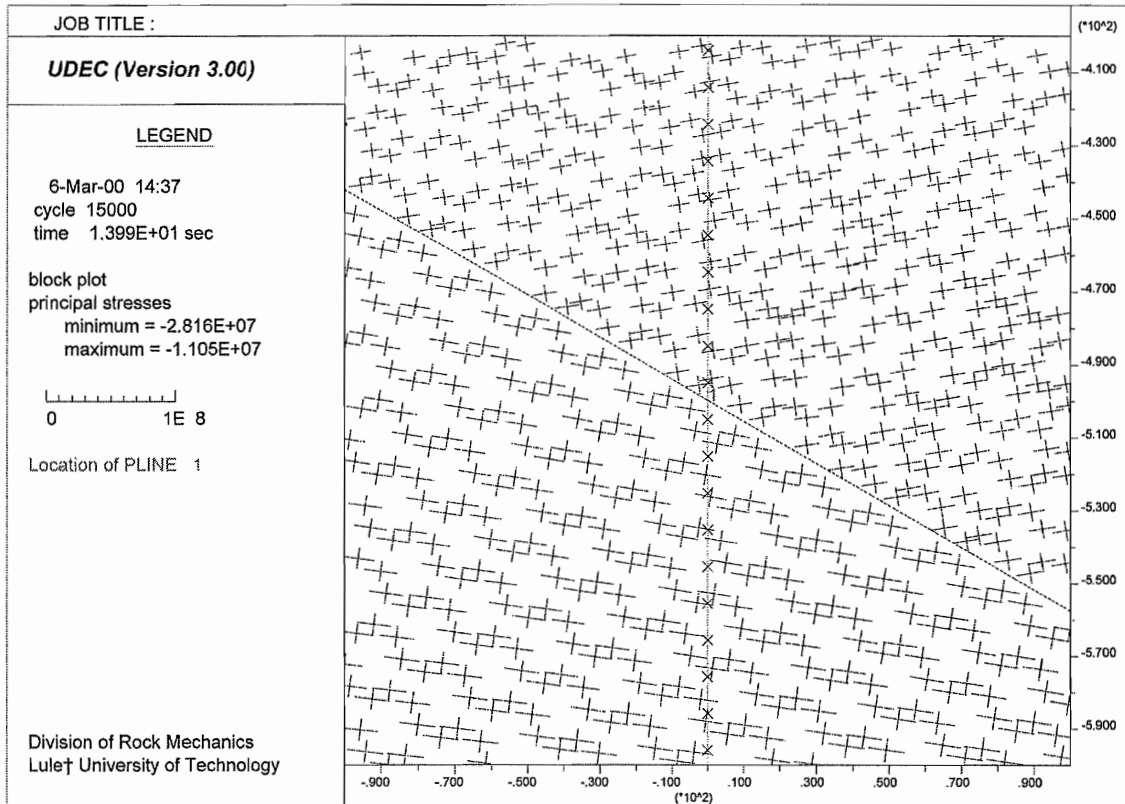
Figure 4-7. *Trajectories of stresses σ_1 and σ_2 near the discontinuity with a dip angle of 30 degrees.*

4.2 Effect of the properties of a thick zone

4.2.1 The model build-up

In this study the discontinuity is simulated as a thick zone of a linear elastic material. The dip angle and the thickness of the zone were set to 30 degrees and 50 meters, respectively, see Figure 4-8. The contacts between the zone and the host rock were simulated as fictitious joints and therefore given high values of the cohesion, friction angle, tensile strength and stiffness.

Totally eight different sensitivity analyses were carried out. In four of them the influence of Young's modulus were studied. In two analyses the influence of Poisson's ratio were studied. The last two analyses were carried out to study the influence of the density. In Table 4-5 the material properties of the discontinuity is presented.
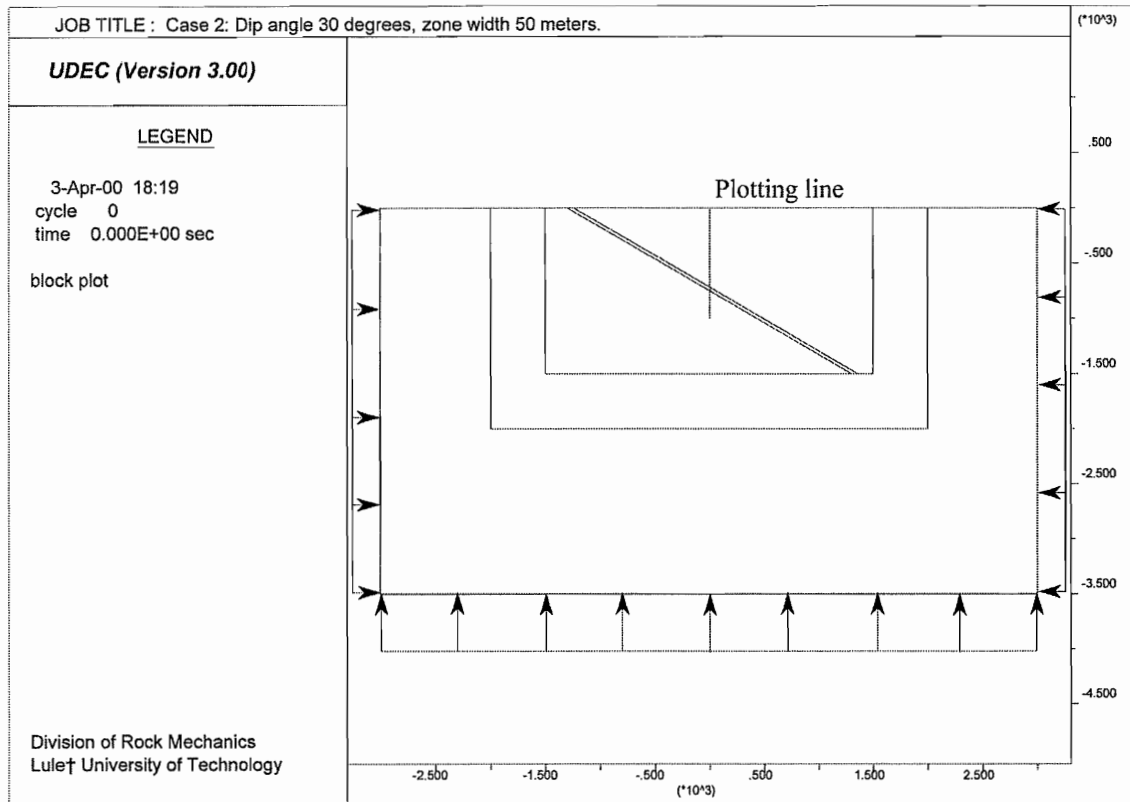
Figure 4-8. *The zone model.*

Table 4-5. **Properties of the discontinuity zone in the different analyses.**

Study parameter	Zone thickness (m)	Young's modulus (GPa)	Poisson's ratio	Density (kg/m³)
	50	40	0.24³	2750
Young's modulus	50	50	0.24	2750
	50	60	0.24	2750
	50	90	0.24	2750
Poisson's ratio	50	73¹	0.15	2750
	50	73	0.30	2750
Density	50	73	0.24	2300
	50	73	0.24	3000

4.2.2 Results

The stresses are plotted along a fictitious vertical line in the model. The plot line intersects the zone at the depth interval between 716 and 750 meters. The stress ratios, R_1 and R_2 are calculated according to Equation (4-3) and can be seen in Table 4-6. The dip angle of the major horizontal stress is measured positive clockwise from the x-axis in the model.

---

[1] Young's modulus and Poisson's ratio of Äspö diorite.

28

Table 4-6.   Stress ratios and the orientation of σ_1 in the zone.

Study parameter	Ratio of σ_1	Ratio of σ_2	Dip angle of σ_1 [°]
Young's modulus			
40 MPa	0.84	0.78	25
50 MPa	0.87	0.87	17
60 MPa	0.92	0.94	9
90 MPa	1.12	1.05	-9
Poisson's ratio			
0.15	0.92	0.94	10
0.30	1.08	1.03	-6
Density			
2300 kg/m^3	1.0	1.0	0
3000 kg/m^3	1.0	1.0	0

In Figure 4-9 the effect of Young's modulus on the stress ratios is shown graphically. The grey zone represents the discontinuity zone in the model. The effect of Poisson's ratio and the density on the stress ratios can be seen in Figures 4-10 and 4-11, respectively. In Figures 4-12 to 4-13 the orientation of σ_l are presented due to different values of Young's modulus, Poisson's ratio and density of the zone.
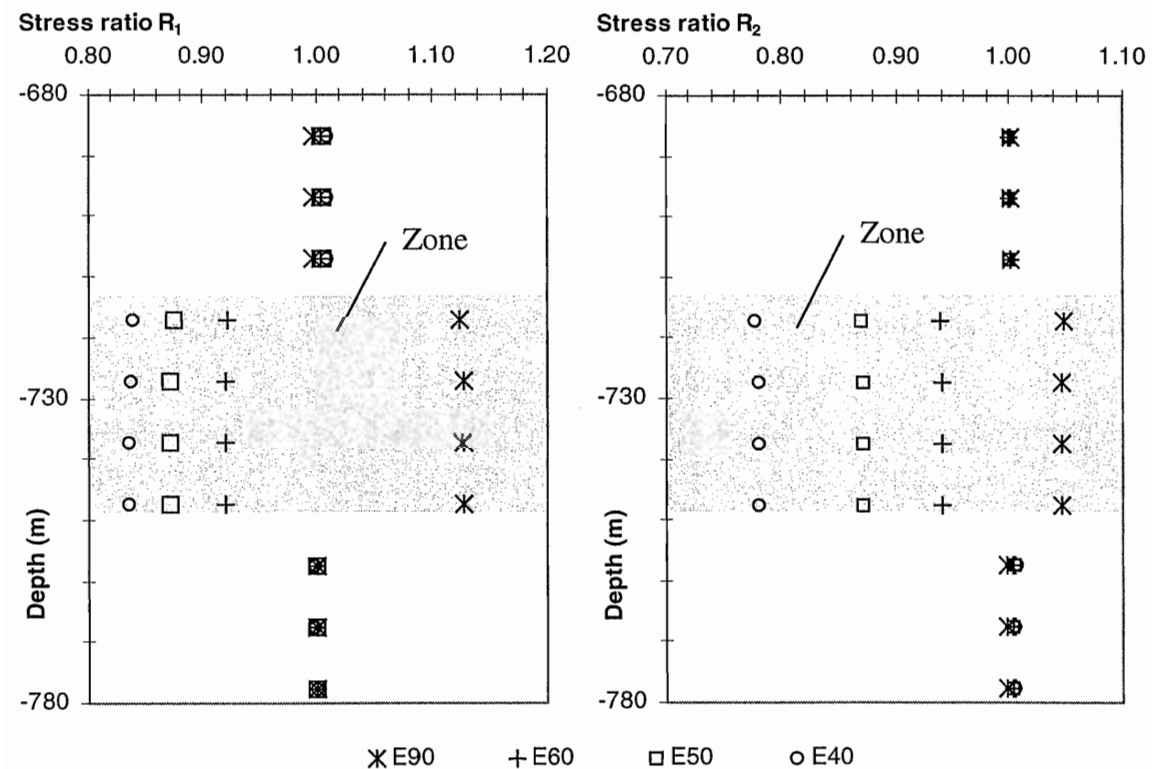
Figure 4-9.   The effect of Young's modulus, E (GPa) on the stress ratios.
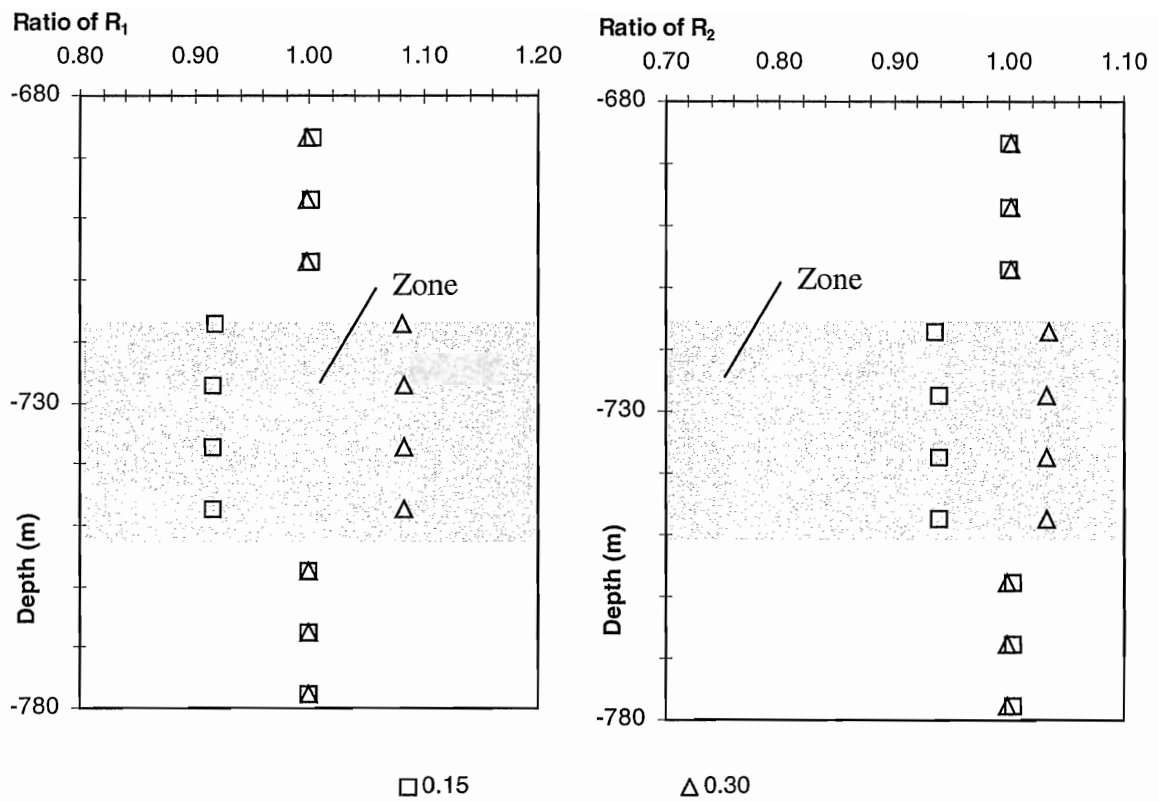
Figure 4-10. *The effect of Poisson's ratio on the stress ratios.*
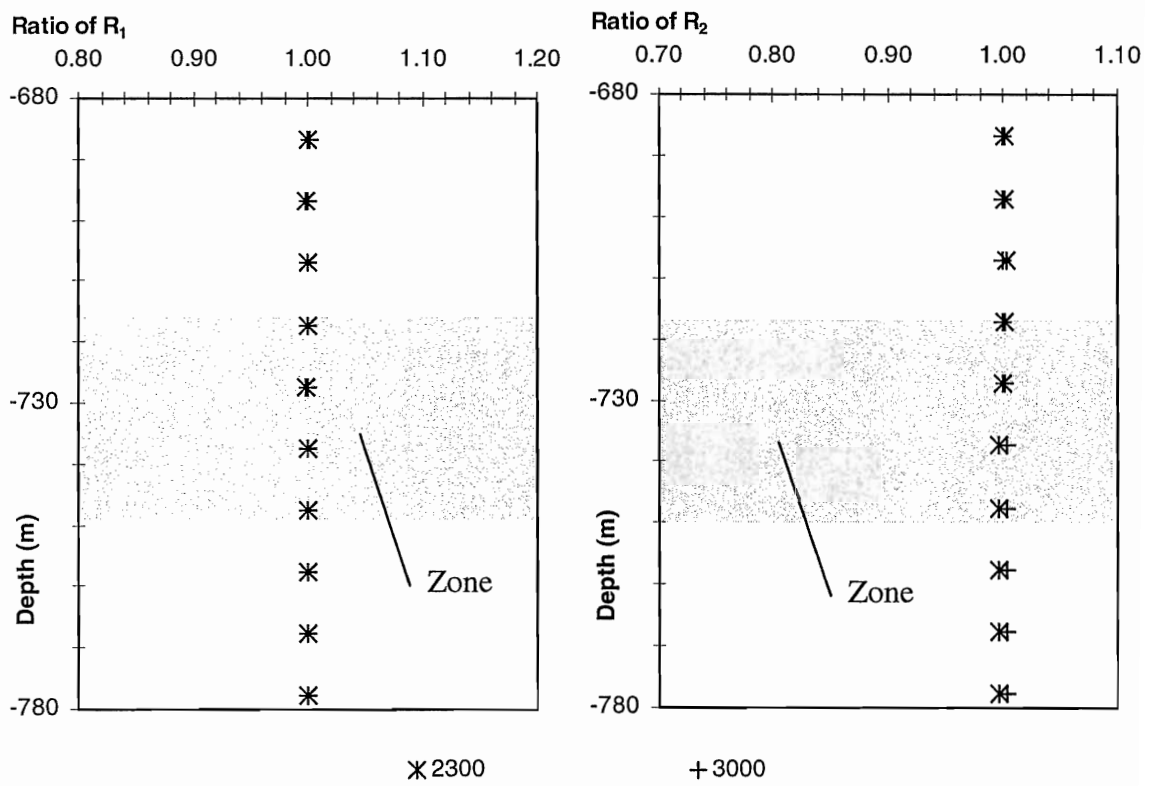
Figure 4-11. *The effect of the density on the stress ratios.*
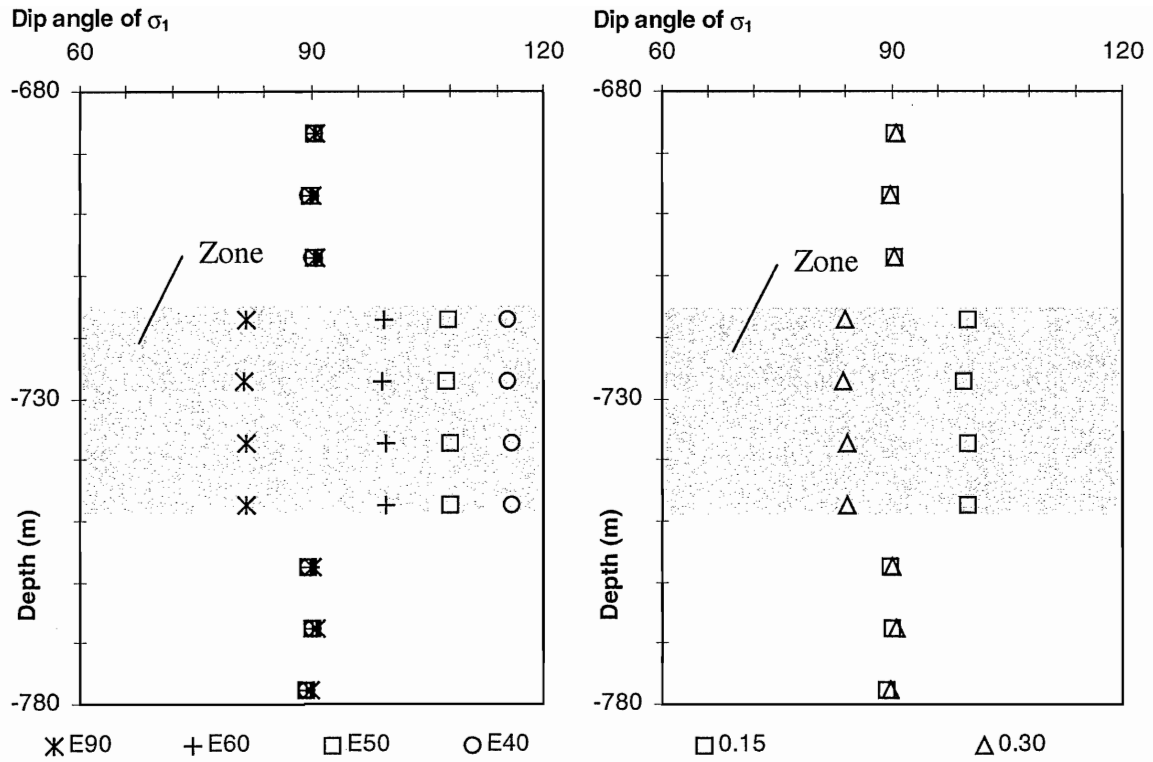
Figure 4-12. *The effect of Young's modulus (a) and Poisson's ratio (b) on the dip angle of σ₁.*
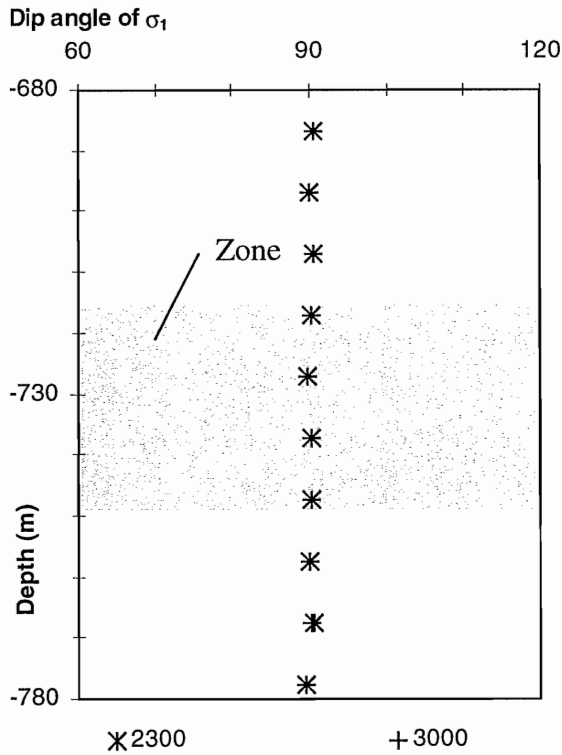
Figure 4-13. *The effect of density on the orientation of σ₁.*

31

4.3   The effect of the stiffness of a discontinuity

The discontinuity zone is simulated as a single discontinuity in this study. The wider the zone the less the value of the normal and shear stiffness of the discontinuity.

4.3.1   The model

In this model (Figure 4-14) the zone is represented by a discontinuity with a dip angle of 30° whose normal and shear stiffness correspond to the mechanical width of the zone.

In an earlier numerical study of the Äspö Hard Rock Laboratory made by Hakami et al, (1998) the following correlation between the width of the joint and joint stiffness were used,

$$jkn = \frac{10}{x} \qquad [GPa/m] \qquad\qquad 4\text{-}5$$

$$jks = \frac{5}{x} \qquad [GPa/m] \qquad\qquad 4\text{-}6$$

where jkn represents the normal stiffness and jks the shear stiffness of the joint and x is the mechanical width of the zone. In Table 4-7 the properties of the discontinuity used in this stiffness model are presented.

Table 4-7.   The properties of the discontinuity due to different mechanical width.

Width of the zone [m]	Jkn [GPa]	Jks [GPa]	Friction	Cohesion	Tension
5	2.00	1.000	10	0	0
10	1.00	0.500	10	0	0
20	0.500	0.250	10	0	0
30	0.333	0.167	10	0	0
40	0.250	0.125	10	0	0
50	0.200	0.100	10	0	0
100	0.100	0.050	10	0	0
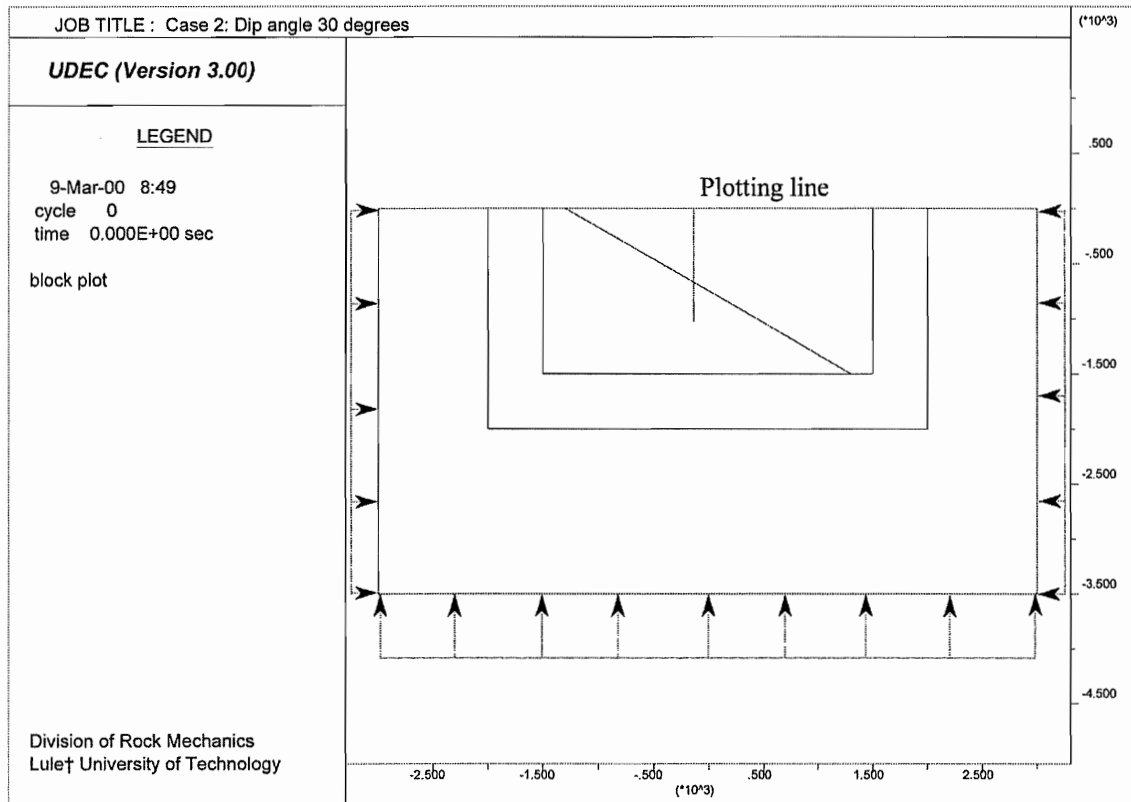
Figure 4-14. The stiffness model.

4.3.2 Results

Figure 4-15 and 4-16 shows the effect of the mechanical width on the principal stresses, while Figure 4-17 illustrate the influence on the orientation of the major principal stress. The intersection between the plotting line and the discontinuity is approximately at a depth of 750 meters. The stress ratios and the orientation of the major principal stress above and below the discontinuity are listed in Table 4-8.

Table 4-8. Stress ratios and orientation of σ_1 in the vicinity of the discontinuity (dip angle 30°).

Mechanical width (m)	Stress ratio, R_1			Stress ratio, R_2			Orientation of σ_1 (°)		
	Above	Below	ΔR_1	Above	Below	ΔR_2	Above	Below	Δ
5	0.8957	1.0643	0.1687	1.0026	1.0869	0.0842	9.33	-8.49	17.82
10	0.8976	1.0615	0.1639	1.0040	1.0856	0.0816	8.92	-8.31	17.23
20	0.8971	1.0612	0.1642	1.0038	1.0855	0.0817	8.99	-8.32	17.31
30	0.8965	1.0610	0.1644	1.0032	1.0855	0.0823	9.04	-8.33	17.38
40	0.8960	1.0607	0.1647	1.0032	1.0850	0.0819	9.09	-8.33	17.42
50	0.8957	1.0603	0.1647	1.0026	1.0851	0.0824	9.10	-8.33	17.43
100	0.8950	1.0574	0.1625	1.0022	1.0835	0.0812	9.06	-8.24	17.30
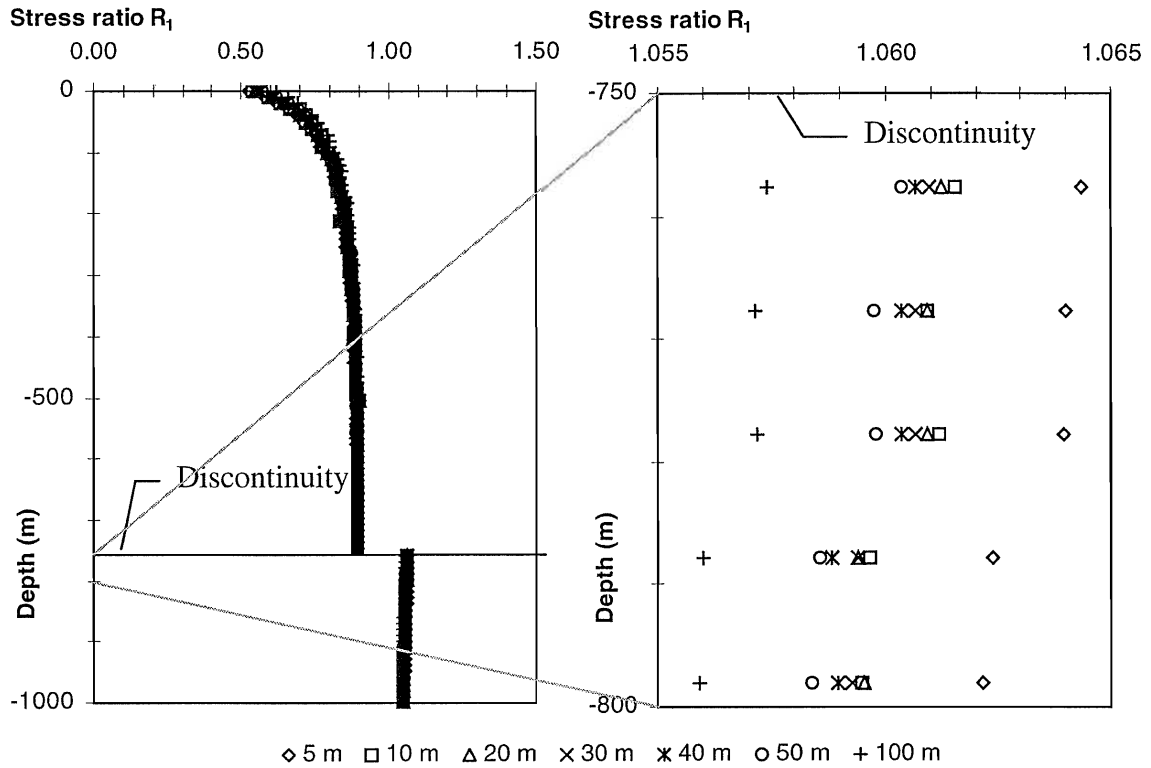
Stress ratio R₁

Figure 4-15. The effect of the stiffness of a single joint on the stress ratio R_1.

Stress ratio R₂

◇ 5 m □ 10 m △ 20 m × 30 m ✳ 40 m ○ 50 m + 100 m
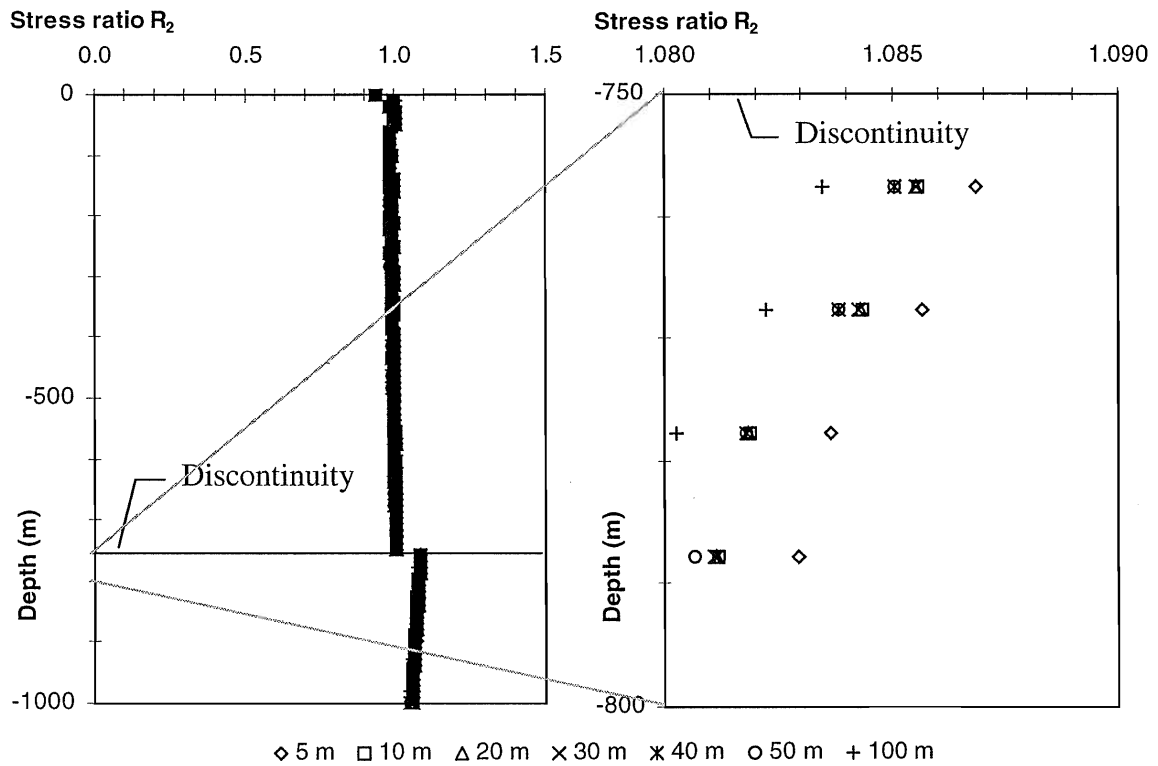
Figure 4-16. The effect of the stiffness of a single discontinuity on the stress ratio R_2.

34
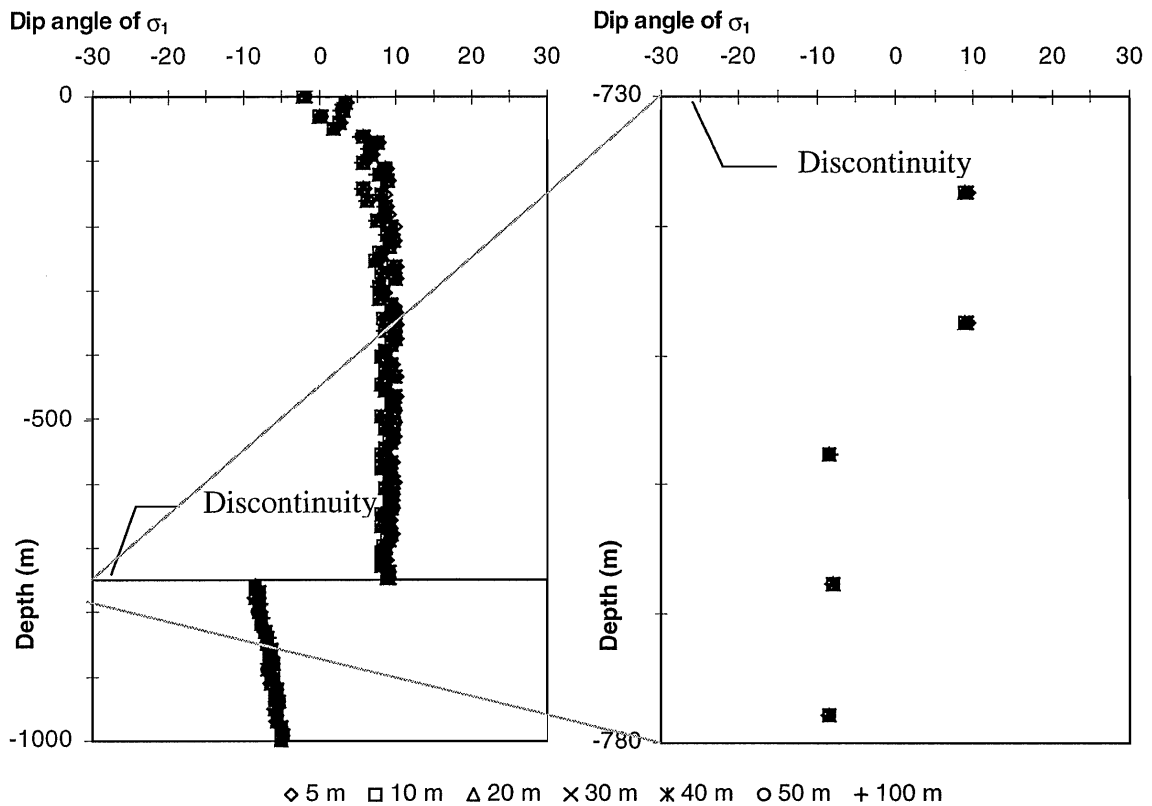
Figure 4-17. The effect of the stiffness on the orientation of the major principal stress.

4.4 The effect of the strength of the zone contacts

4.4.1 The model

This model is a combination of the models presented in 4.2 and 4.3, i.e. a thick zone with low strength contacts (Figure 4-18). The mechanical properties of the zone and the contacts are summarised in Table 4-9. The properties of the contacts were corresponding to the properties of zone with the mechanical width of 5 meters.

Table 4-9   Rock properties used in the stiffness model.

Mechanical Parameters	Value
Zone rock	
Density	2750 kg/m^3
Young's modulus	40 GPa
Poisson's ratio	0.24
True joints	
Joint normal stiffness	2·10^9 Pa
Joint shear stiffness	1·10^9 Pa
Joint friction	10°
Joint cohesion	0 Pa
Joint tension	0 Pa

35

JOB TITLE : Case 2: Dip angle 30 degrees, zone width 50 meters.

UDEC (Version 3.00)

LEGEND

3-Apr-00 18:19
cycle 0
time 0.000E+00 sec

block plot

Division of Rock Mechanics
Luleå University of Technology
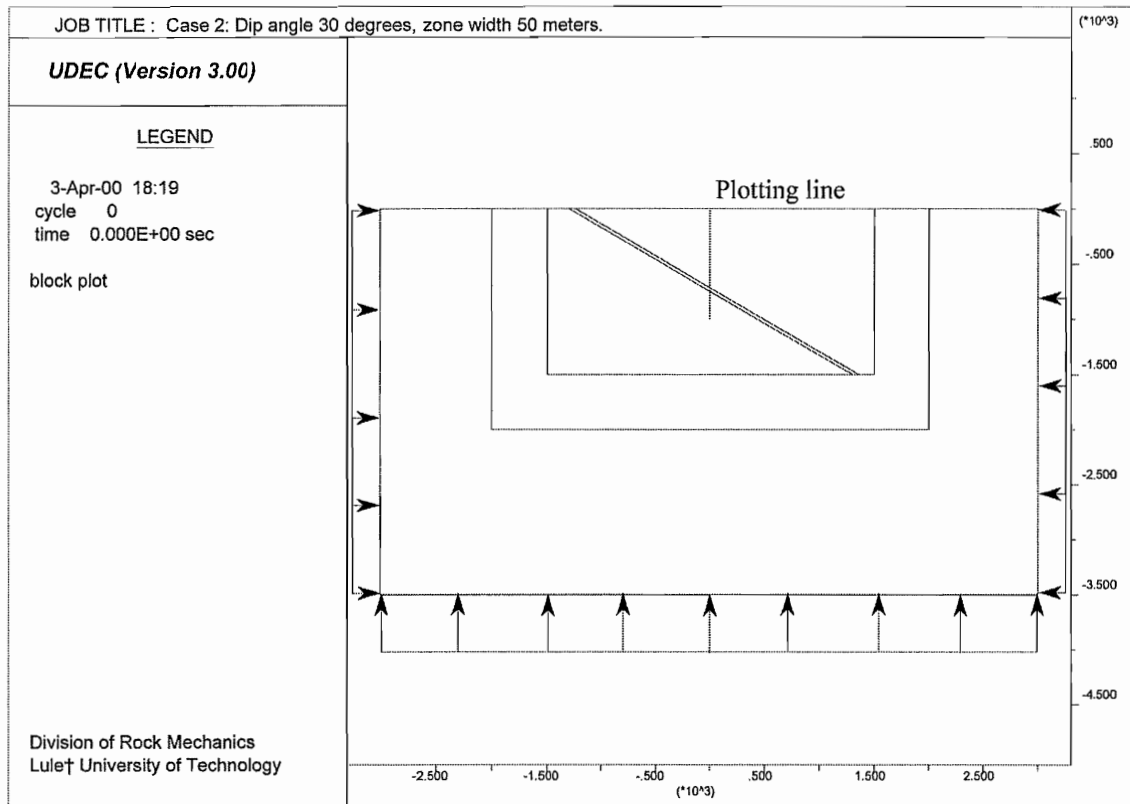
Figure 4-18. The zone model.

4.4.2 Results

The results are presented in combination with the results from section 4.3 ($E = 40$ GPa and $v = 0.24$). Figure 4-19 shows the stress ratios and Figure 4-20 shows the orientation of σ_1. Both the stress magnitudes and orientations are now affected outside the zone as a result of the shear movements that occur in the soft low strength contact. The stress ratios in the soft contact model above and below the zone are the same as for the model with a single discontinuity with properties corresponding to a zone with the mechanical width of 5 meters.

36
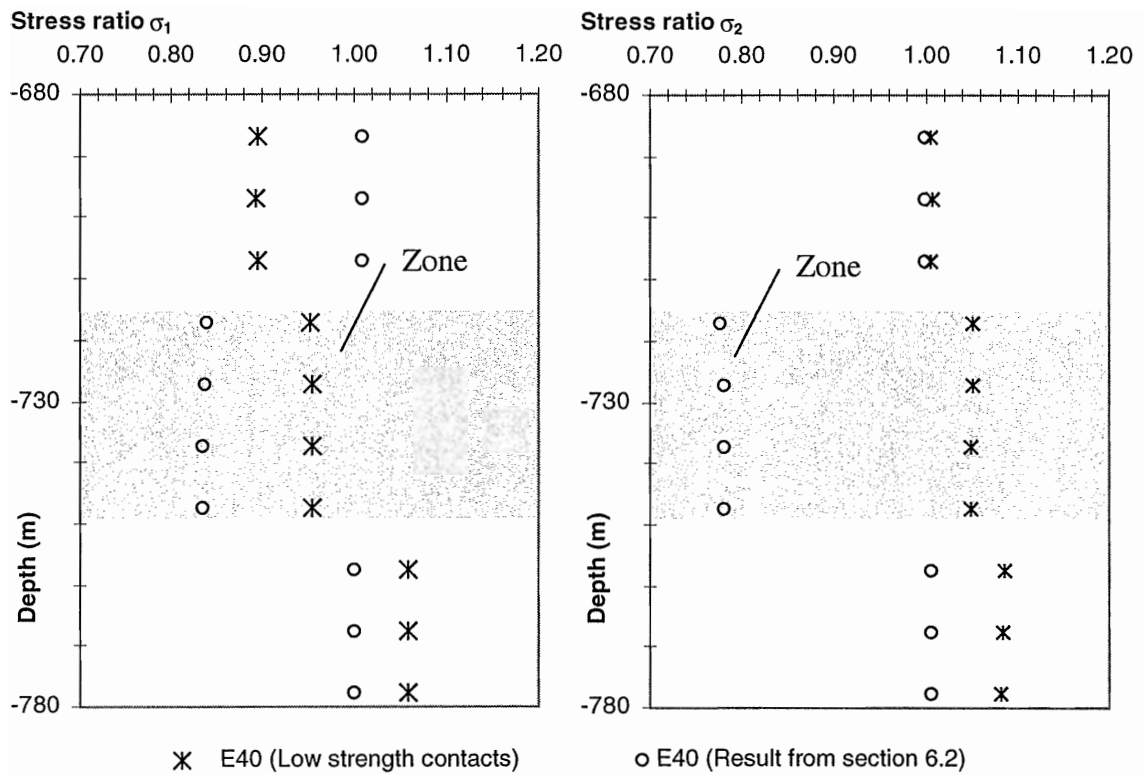
Figure 4-19. *The comparison between the stress ratios R_1 and R_2 in a soft and stiff contact model.*
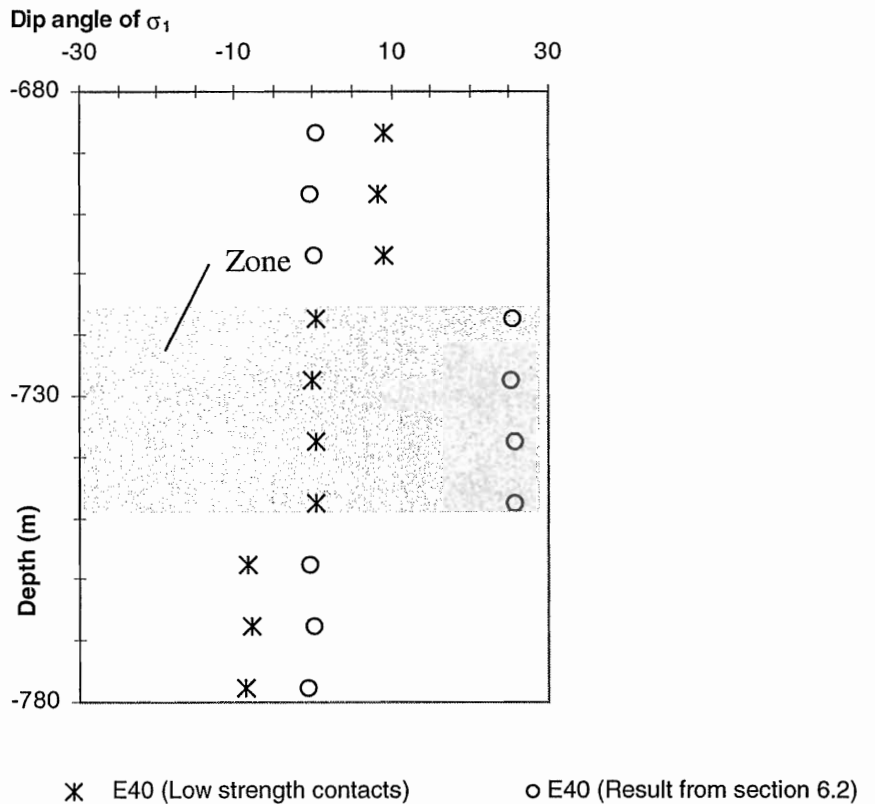
Figure 4-20. *The comparison between the orientation of the major principal stresses in a soft and stiff contact model.*

37

4.5   Discussion

4.5.1   Effect of the dip of the discontinuity

An inclined discontinuity influences the stresses more or less depending on the dip angle. The major principal stress is more influenced at a dip angle of 30° than 45° whereas the opposite is true for the minor principal stress, for a friction angle of 10 °. It could also be stated that the major principal stress is mainly affected on the side above the discontinuity, while the opposite is true for the minor principal stress.

However, it is clear that the stresses re-distribute near the discontinuity. The stresses orient themselves to tend to be parallel and perpendicular to the discontinuity depending on if the discontinuity is softer or stiffer than the host rock.

4.5.2   Effect of the properties of the zone

The analyses of the zone with elastic material properties and contacts that are stiff showed that the properties of the zone are affecting the stresses within the zone. However, it is possible that if a smaller mesh size had been used in the area near the discontinuity, stress changes may be visible even outside the zone. The simulation results showed that a zone with higher Young's modulus concentrates the stresses to the zone. The stresses in the zone will then be higher than if a lower value of the Young's modulus was used. The similar phenomenon occurs for a higher value of Poisson's ratio, while the density of the zone, hardly affects the stresses at all.

The orientation of the major principal stress is affected by the elastic properties within the zone. The major principal stress is horizontal on both sides of the zone. When Young's modulus of the zone is lower than Young's modulus of the side rock the orientation of the major principal stress becomes more parallel to the dip angle (30°) of the zone, see Figure 4-21. For a higher Young's modulus, σ_l becomes more perpendicular to the dip angle of the zone (Figure 4-22). This seems to coincide with the result reported by Hudson and Cooling (1988). The same phenomenon occurs when the Poisson's ratio is lower (parallel) and higher (perpendicular) than the side rock. The orientation, however, seems to be unaffected by the density of the rock in the zone, at least when the density is within the range of 2300 - 3000 kg/m^3.

There is almost no indication of an existing zone from the stresses in a point in the vicinity of the zone. The reason for why almost no stress changes are seen in the vicinity is probably because no shear movements occur along the zone.
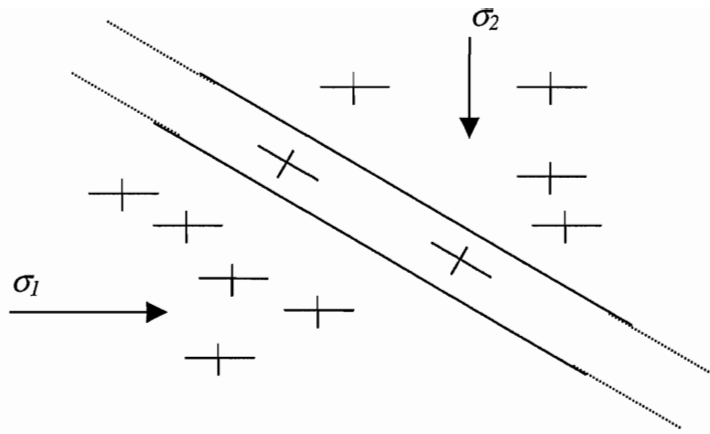
Figure 4-21. *Re-orientation of the principal stresses due to lower Young's modulus and Poisson's ratio than the host rock.*
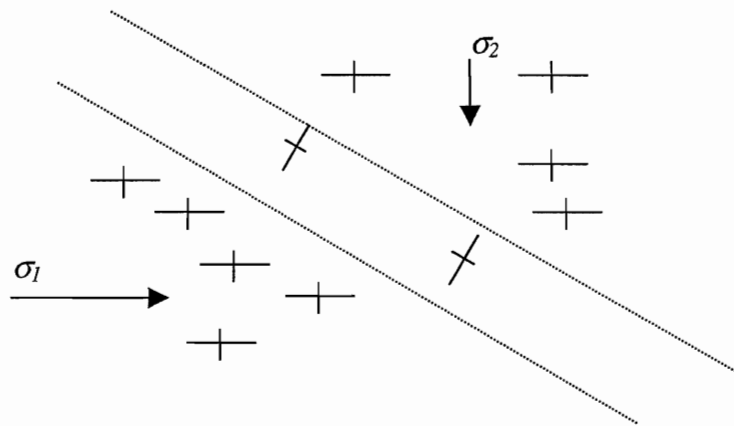
Figure 4-22. *Re-orientation of the principal stresses due to higher Young's modulus and Poisson's ratio than the host rock.*

4.5.3 The effect of the normal and shear stiffness of the discontinuity

The stress magnitudes are more or less unaffected in the tested interval of the normal and shear stiffness of the discontinuity. However, it could be shown from the results that a discontinuity with higher normal and shear stiffness (i.e. a narrower zone) resulted in slightly higher stresses.

On the other hand, the friction angle of the discontinuity influences the results far more than the stiffness as illustrated in Figure 4-2.

4.5.4 The effect of soft low strength contact of a thick zone

The numerical analyses showed that when the strength of the contacts between the discontinuity zone and the host rock is low, shear movements occurred. Due to this sliding, the rock stresses redistribute around and inside the zone. The stresses obtained outside a 50 metre thick zone with low strength contacts corresponding to a mechanical width of 5 meters is equal to the stresses outside the discontinuity with normal and shear stiffness corresponding to a mechanical width of 5 m (see Table 4-8).

39

4.6 Conclusion

Conclusions regarding both physical phenomena and modelling techniques are listed below starting with the physical.

- The stresses are affected by the dip angle of the discontinuity, but there is no consistent correlation between the stress magnitudes and the dip angle.

- The stresses are affected when shear movements occur along the discontinuity.

- The stresses in the vicinity of the discontinuity change barely when the normal and shear stiffness of the discontinuity varies (i.e. when the width of the discontinuity zone varies).

The following conclusions are more concerned with the modelling technique, even if they also have a physical meaning.

- The influence of the stresses in the vicinity of a wide zone is mainly governed by the high strength of the contacts of the zone. Using high shear strength contacts hardly any shear movements occur along the contacts resulting in only stress changes (magnitudes and orientation) within the zone. If the contacts of the zone instead would have been modelled with low strength contact, sliding occurs in the contacts and a change in the stresses on both sides of the zone may be induced.

- Simulating the zone as a single discontinuity, which the normal and shear stiffness are correlated to the mechanical width, the stresses will be influenced on both the sides of the discontinuity.

The major conclusion of these analyses will be used in the 3D model, namely that the major discontinuities can be simulated with normal- and shear stiffness that corresponds to the mechanical widths of the major discontinuities.

40

5 3d-analysis of stresses and its influences of major discontinuities

In this study the eight major structures at Äspö outlined by Rhén et al (1997b) were included in a three-dimensional model of Äspö HRL. The computer code *3DEC* developed by Itasca (1998b) was used in this study.

5.1 3DEC model

The model is divided into three regions in order to use small zones in the area of interest and still not obtain a model with too long calculation time, see Figure 5-1. The different regions are generated with an edge length of 50 m (I), 150 m (II) and 500 m (III).
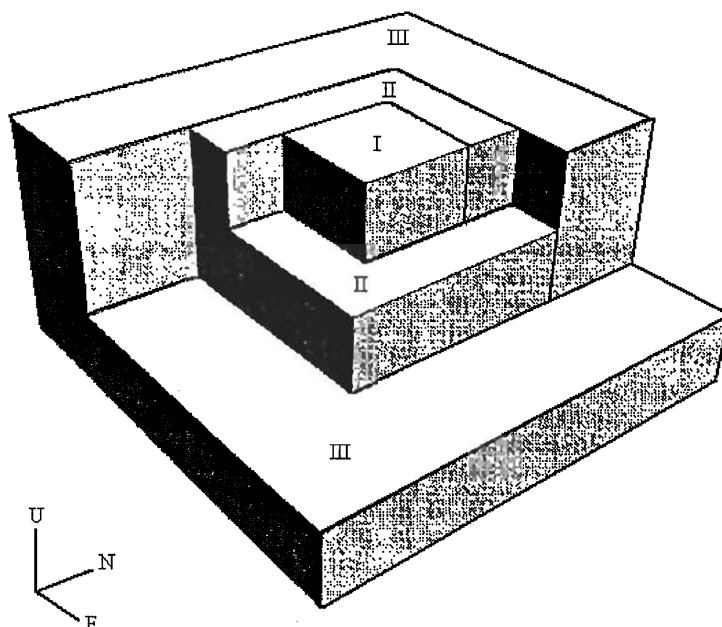
Figure 5-1. *The geometry and the discrete regions of the 3DEC model.*

In the model, the axes *north*, *east* and *up* are represented by the z-, x- and y-axes, respectively.

The conclusions drawn from the 2D analyses have been used during the development of the 3D model. The major geological structures are modelled as single discontinuities with normal and shear stiffness corresponding to the mechanical width of the structures. The reasons for this are two. Firstly, the 2D generic models showed that the stress changes outside a discontinuity zone is the same whether the discontinuity zone is generated as a thick zone with low strength contacts or as a single discontinuity. The second reason is that discontinuities consisting of a zone will result in very complex models especially at intersections, which can cause long calculation time.

The model is oriented so that the stresses initiated in the model will act as compressive normal stresses. At Äspö the orientation of the maximum horizontal stress has a trend of NW-SE. In order to obtain normal stresses on the boundaries of the model, the local

41

north in 3DEC is rotated with respect to magnetic north by 45 degrees (Figure 5-2) around the y-axis.
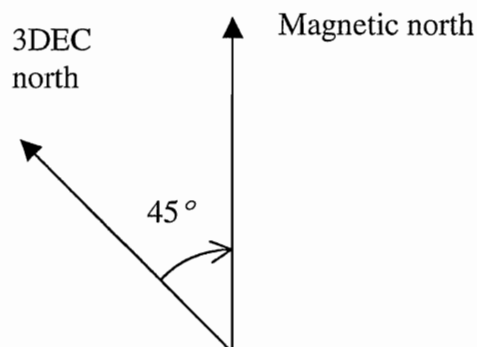
Figure 5-2. *The relationship between the magnetic north and the local north in 3DEC.*

When using this local co-ordinate system, all co-ordinates have to be transformed since the location of the structures and the boreholes are given with respect to the Äspö co-ordinate system. Figure 5-3 shows the transformation of co-ordinates involving pure rotation.
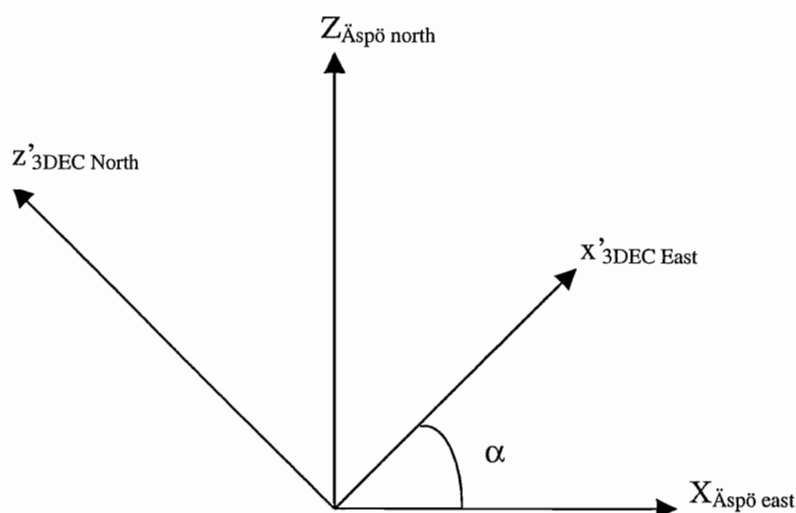
Figure 5-3. *Transformation model.*

The transformation is made according to following equations, Spiegel (1968).

$$x' = x\cos\alpha + z\sin\alpha \qquad\qquad 5\text{-}1$$

$$z' = -x\sin\alpha + z\cos\alpha \qquad\qquad 5\text{-}2$$

The angle, α, between the Äspö co-ordinate system and the 3DEC co-ordinate system is 33 degrees. The major discontinuities at Äspö are determined in three points in the Äspö co-ordinate system (Rhén et al, 1997). To include a discontinuity in 3DEC at least one point on the discontinuity, the dip direction and the dip angle must be known. The point on the discontinuity and the dip direction must be transformed to the new co-ordinate system. In Table 5-1 the results of the transformation of the co-ordinates for the major

Äspö discontinuities are shown. Figure 5-5 shows the model including the discontinuities.

Table 5-1. The co-ordinates of the major discontinuities according to Äspö co-ordinate system (Rhén et al, 1997) and 3DEC co-ordinate system. The orientation of the structures is presented with reference to north in 3DEC.

Structure	Branch	Äspö			3DEC			Strike/Dip
		E (x)	Up (y)	N (z)	E' (x')	Up (y)	N' (z')	(3DEC North)
EW-7	A	2200	-232	6428	5346	-232	4193	210 / 75
NE-4	A	2198	-225	6440	5351	-225	4204	185 / 60
	B	2170	-232	6480	5349	-232	4253	185 / 60
NE-3	A	2095	-233	6610	5357	-233	4403	075 / 75
	B	2076	-222	6650	5363	-222	4446	075 / 75
NE-1	A	2055	-689	7135	5609	-689	4865	080 / 70
	B	2083	-708	7081	5604	-708	4804	080 / 70
EW-3	A	2167	-542	7010	5635	-542	4699	210 / 75
NE-2	A	2083	-349	7250	5696	-349	4946	165 / 70
EW-1	A	2000	-327	7575	5803	-327	5264	180 / 82
	B	2111	-370	7500	5855	-370	5140	180 / 82

5.2 *In situ* stress

In the analysis, three different stress states were used, see Table 5-2. The major horizontal stress is acting in the direction of the z-axis and the minor horizontal stress is acting in the direction of the x-axis.

Table 5-2. The state of stresses[1] used for modelling of the three different cases.

Case	Based on	σ_x (MPa)	σ_z (MPa)	Depth interval (m)
Äspö Bilinear	Compilation of rock stress measurements at Äspö (Lundholm, 2000)	1.4 + 0.034y	2.1 + 0.014y	0 – 450
		-33.2 + 0.11y	-18.1 + 0.06y	450 – 1000
Hydraulic fracturing	Hydraulic fracturing (Amadei and Stephansson, 1993)	2.8 + 0.04y	2.2 + 0.024y	0 – 1000
Overcoring	Leeman-type overcoring (Amadei and Stephansson, 1993)	6.7 + 0.04y	0.8 + 0.033y	0 – 1000

---

[1] Positive stress is compressive

5.3   Mechanical properties

The relationships between the mechanical width and the joint normal and shear stiffness are defined by equations 4-5 and 4-6. In Table 5-3, *jkn* and *jks* for the different discontinuities at Äspö are presented.

Table 5-3.   The mechanical width of the structures at Äspö.

Structure	Branch	Mechanical width (m)	jkn (GPa/m)	jks (GPa/m)
EW-7	A	10	1.000	0.500
NE-4	A	20	0.500	0.250
	B	21	0.476	0.238
NE-3	A	25	0.400	0.200
	B	24	0.417	0.208
NE-1	A	33	0.303	0.152
	B	28	0.357	0.179
EW-3	A	14	0.714	0.357
NE-2	A	6	1.667	0.833
EW-1	A	100	0.100	0.050
	B	100	0.100	0.050

The rest of the rock properties used in the model are listed in Table 5-4. The value of the friction angle was chosen based on the filling/material of the discontinuities. Most of them had material such as clay, mylonite, clay altered rock, wide crushed and a few of them were consecutively. In a paper by Barton (1973) a review was made on the shear strength of filled discontinuities in rock for rocks like diorite, the clay-filled discontinuities had a peak friction angle of 26°. Based on this, the friction angle in the study was set to 20°.

Table 5-4.   Rock properties used in the 3DEC model.

| Parameter	Value
Joint normal stiffness	Depending on the mechanical width of the zone (Table 5-3).
Joint shear stiffness	Depending on the mechanical width of the zone (Table 5-3).
Joint friction	20°
Joint cohesion	Zero
Joint tension	Zero
Young's modulus of host rock	73 GPa
Poisson's ratio of host rock	0.24
Density of host rock	2750 kg/m^3

5.4   Boundary conditions and model geometry

During the development of the optimal model geometry and boundary conditions several ideas have been discussed.

The discontinuities should not intersect the boundaries of the model due to both physical and modelling reasons. All discontinuities in the earth crust, regardless of the size are finite and enclosed by rock. Sliding along a discontinuity can, therefore, not occur without interaction with the surrounding rock. So, models completely intersected by discontinuities will not reflect the physical behaviour of the earth crust. Furthermore, an almost infinitesimal slip along a discontinuity, which completely intersects a model, will give rise to an unbalance, inducing rotation and additional slip. Therefore, the discontinuities, representing the major geological structures at Äspö HRL, will not completely intersect the model, see Figure 5-4. Vertical and horizontal impenetrable blocks with a thickness of 200 and 500 m thick, respectively, are used to enclose the discontinuous model of Äspö.

The interest here is not to simulate the whole build-up of the stresses in the earth crust over billions of years including the geological processes, the periods with and without land ice and the stress relaxation processes. The stresses are therefore, initiated in the model where the intact material and the discontinuities are given the actual values of the elastic parameters. The model is then run to equilibrium. Then the discontinuities were given the actual strength values and the model was again run to equilibrium.

Horizontal view   Vertical view

Figure 5-4.   A model outline with the impenetrable blocks.

5.5   Model of Äspö

The model of Äspö is illustrated in Figure 5-5. The boundaries are fixed and the assumed virgin stresses are initiated in the whole model. The same modelling sequences were made for the three different analysed states of stress. First the discontinuities were given extreme high cohesion and tensile strength forcing the material to behave elastically and rapidly achieves the stress distribution in the model. After the model reached the equilibrium the cohesion and tensile strength were set to the actual values. Finally, the model was cycled until equilibrium was achieved.

Two comparative analyses were made in order to study if the results are depending on how the discontinuities are generated. In the first of these two analysis all discontinuities were given theirs actual cohesion, tensile strength, normal and shear stiffness at the same time and in the other analysis the discontinuities were given their actual strength one by one

45
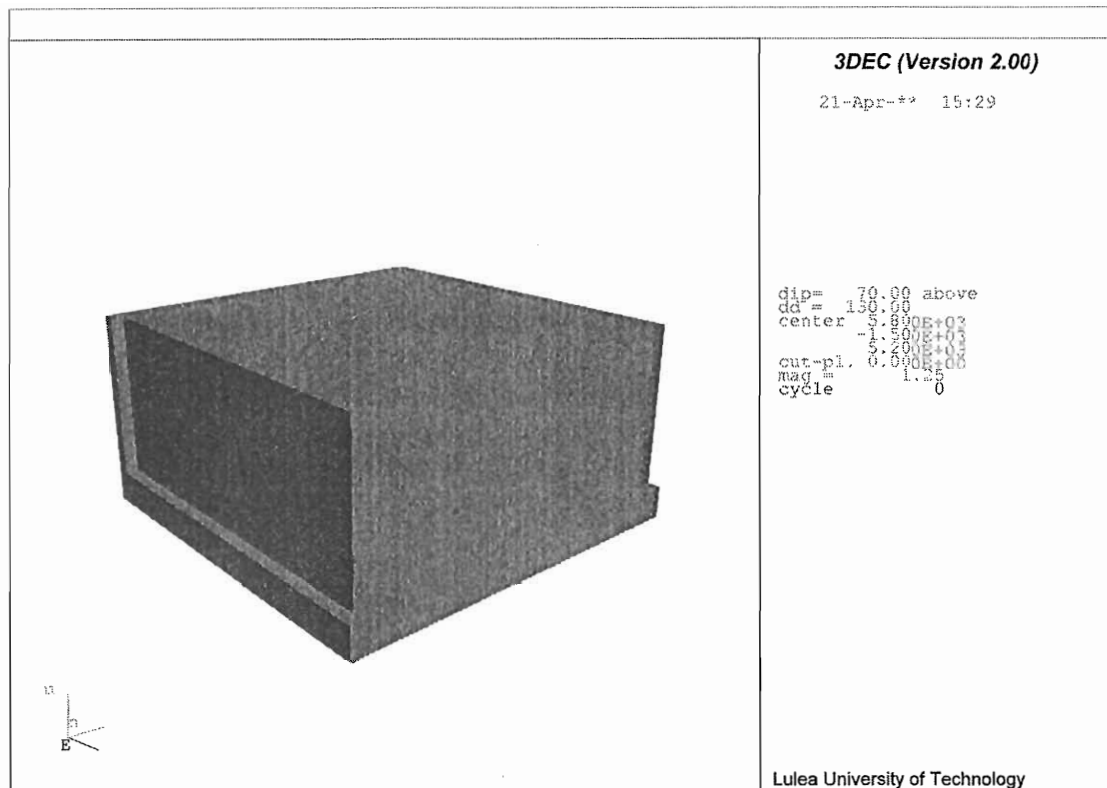
Figure 5-5. *The 3DEC model including the discontinuities, the solid blocks are hidden*

5.6   Stress measurements at Äspö

The results from the numerical analyses are compared to some of the stress measurements made at Äspö. The chosen boreholes are KAS02, KAS03, KAS05 (Bjarnason et al, 1989) and KXZSDS8HL (Ljunggren and Klasson, 1996). Information about the boreholes is given in Table 5-5. The results from the stress measurements in these boreholes at Äspö are summarised in Appendix A (KAS02, KAS03 and KAS05) and Appendix B (KXZSDS8HL).

Table 5-5.   Information about rock stress measurement boreholes.

Borehole	Measurement technique	Start location in the model			Stop location in the model		
		N	E	Depth	N	E	Depth
KAS02	Hydraulic fracturing	4933	5738	0	4933	5738	-800
KAS03	Hydraulic fracturing	5523	5739	0	5523	5739	-1000
KAS05	Overcoring SSPB Cell	4957	5675	0	4957	5675	-500
KXZSDS8HL	Overcoring CSIRO HI Cell	4872	5855	-416	4843	5850	-411

5.7   Results

The stresses calculated using 3DEC, the three different virgin stress states and the measured stresses are illustrated together for each borehole. The stresses are evaluated from the model by plotting the stresses along a line that represent the centre line of a borehole. The major and minor horizontal stresses for the boreholes KAS02, KAS03, KAS05 and KXZSD8HL are shown in Figures 5-6 to 5-13. The solid lines in the figures presenting the magnitudes of the horizontal stresses represent the 80% and 120% of the

46

measured stress in the borehole. In Figure 5-14 to 5-17 the orientation of the maximum horizontal stress are presented and the solid lines correspond to the orientation ± 15 degrees.

Since the principal stresses are more or less horizontal and vertical there is no interest in comparing these with the measured principal stresses in KAS05 and KXZSD8HL.

Analyses were carried out in order to investigate if the state of stress was affected by the way the discontinuities were introduced in the model. These analyses showed that the stresses and the displacements in the model are the same after equilibrium, weather all discontinuities were generated at the same time or one by one.
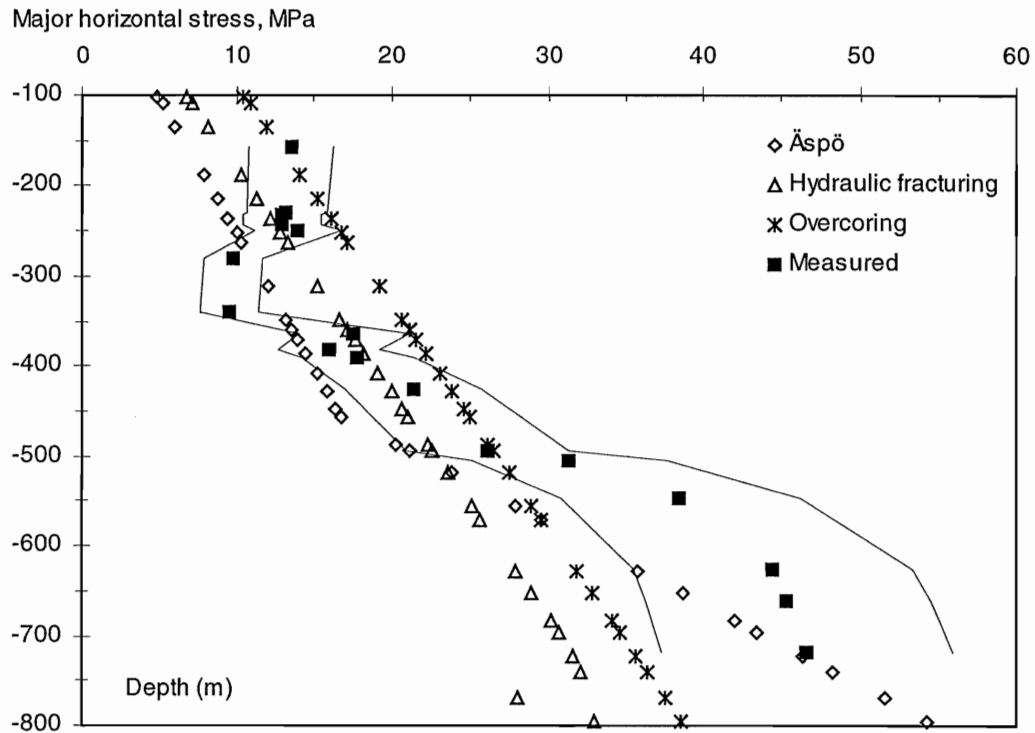
Figure 5-6.   *The major horizontal stress in KAS02.*

47
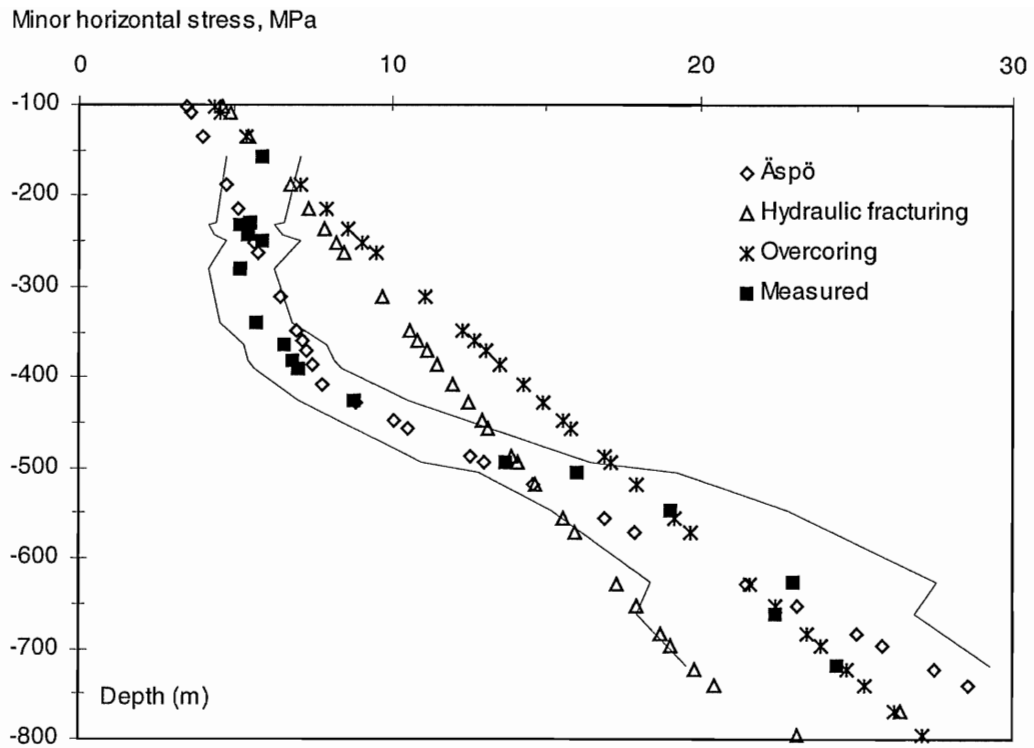
Figure 5-7. *The minor horizontal stress in KAS02*
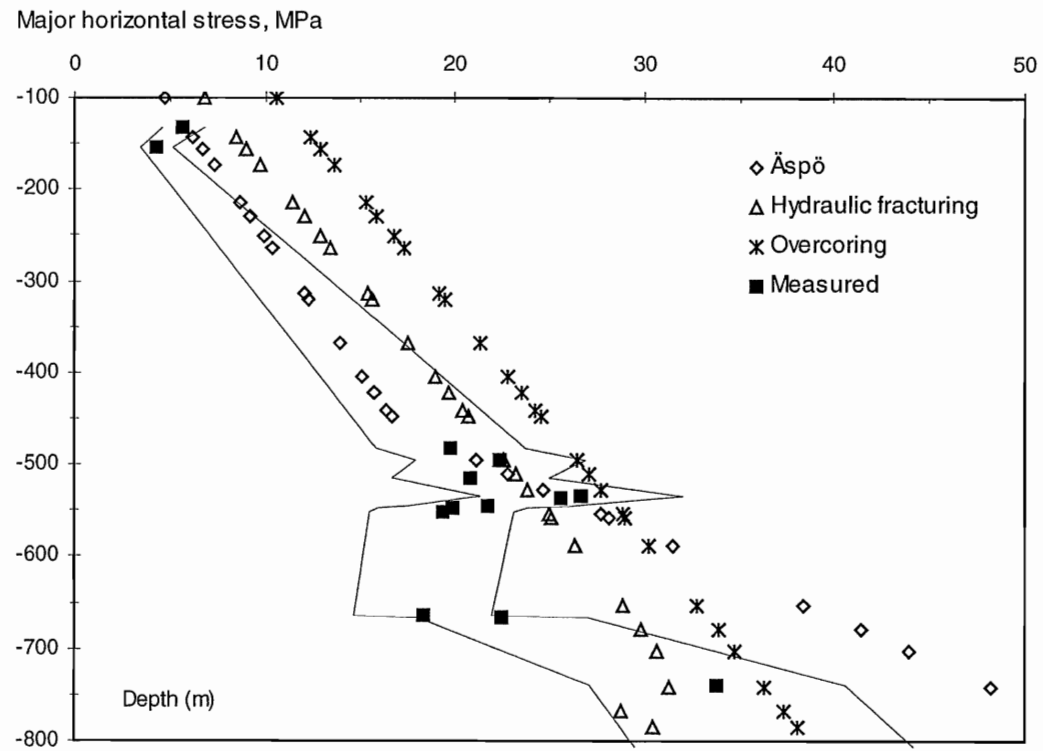
Figure 5-8. *The major horizontal stress in KAS03.*

48
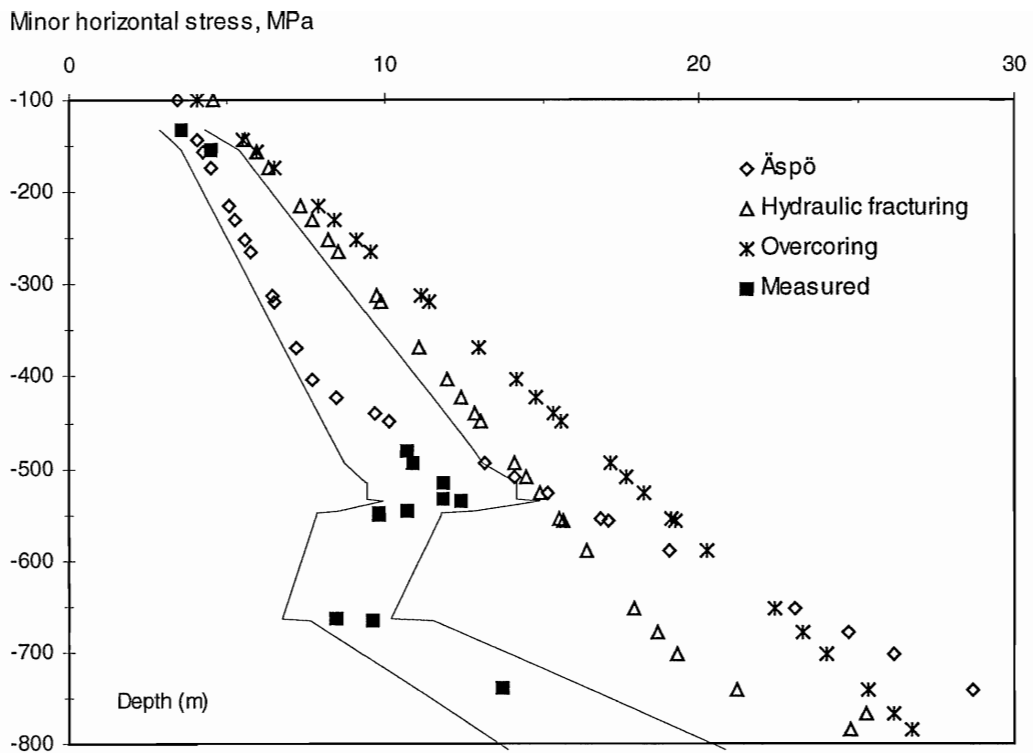
Figure 5-9. *The minor horizontal stress in KAS03.*
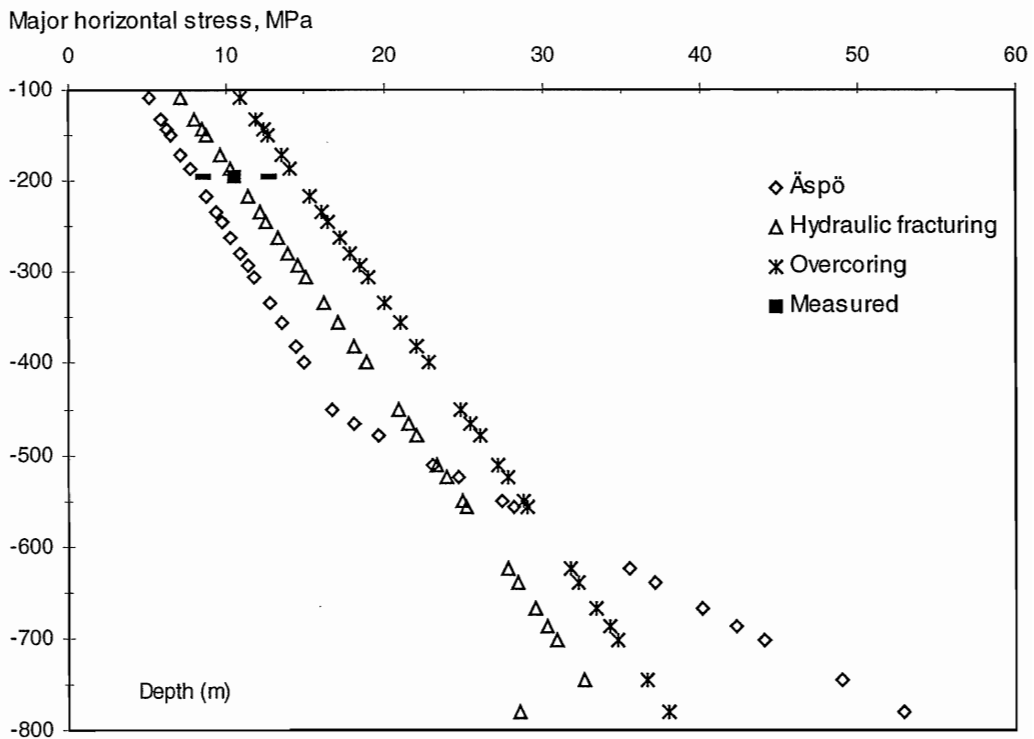
Figure 5-10. *The major horizontal stress in KAS05.*

49
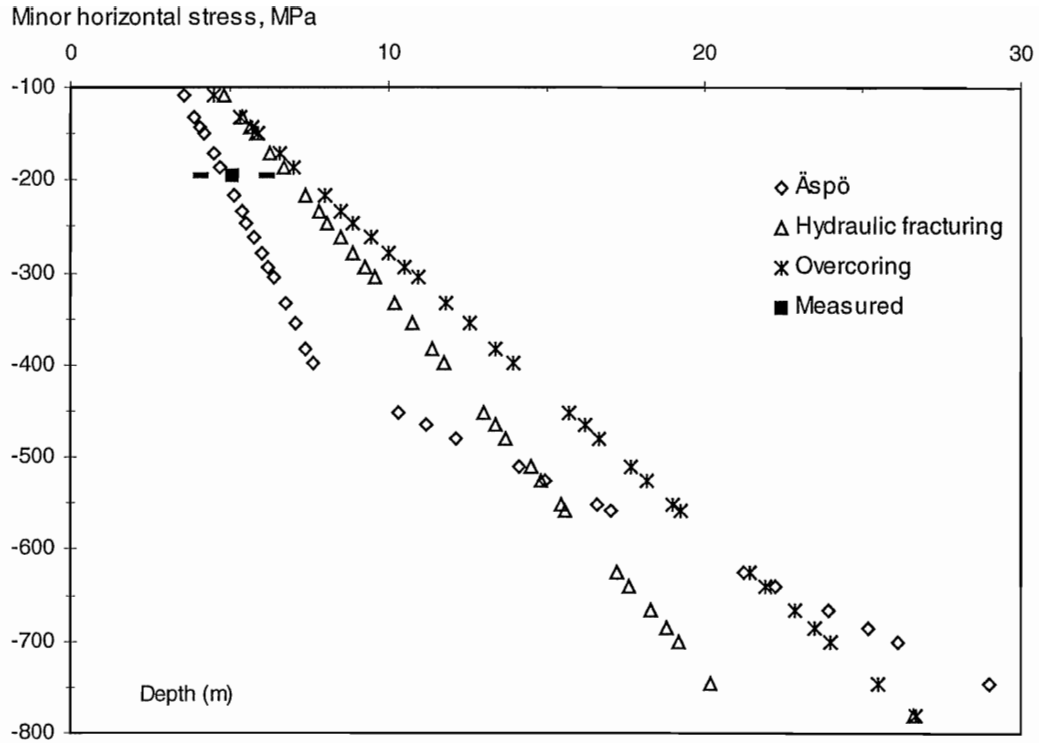
Figure 5-11. *The minor horizontal stress in KAS05.*
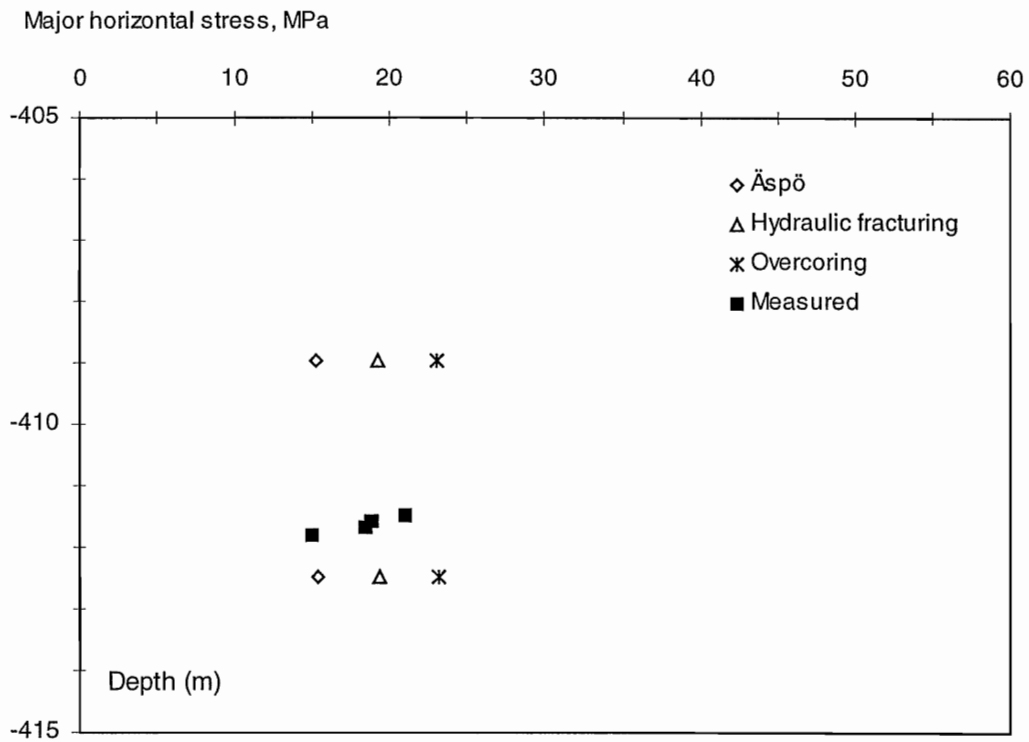
Figure 5-12. *The major horizontal stress in the horizontal borehole KXZSD8HL.*

50

Minor horizontal stress, MPa
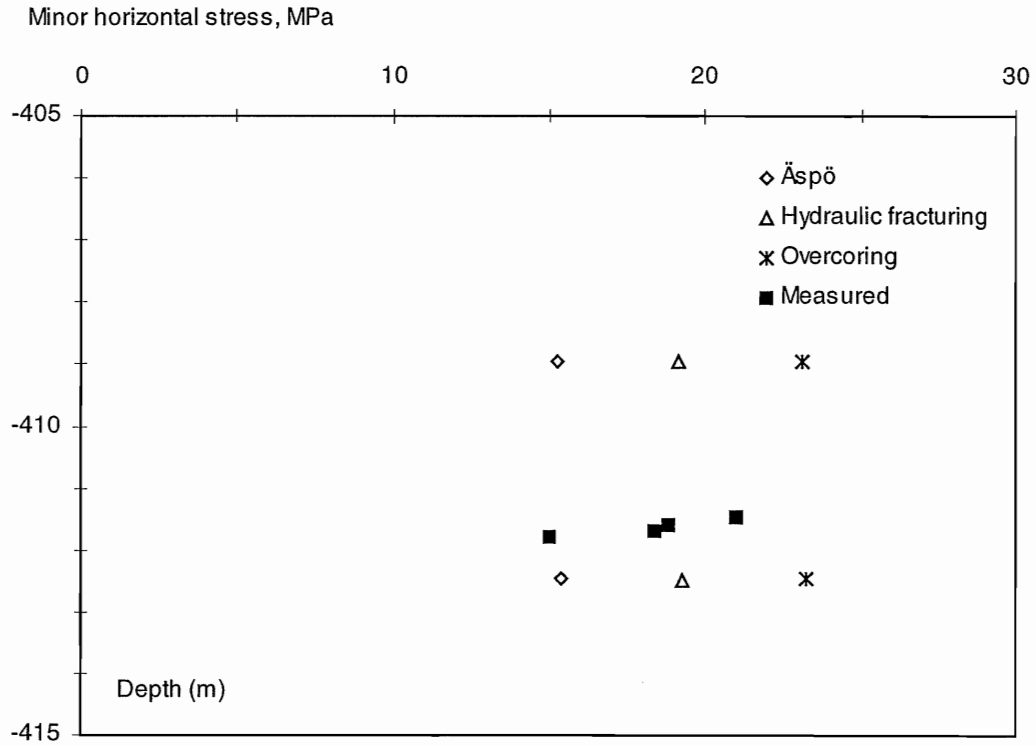
Figure 5-13. *The minor horizontal stress in the horizontal borehole KXZSD8HL.*

Orientation of the major horizontal stress
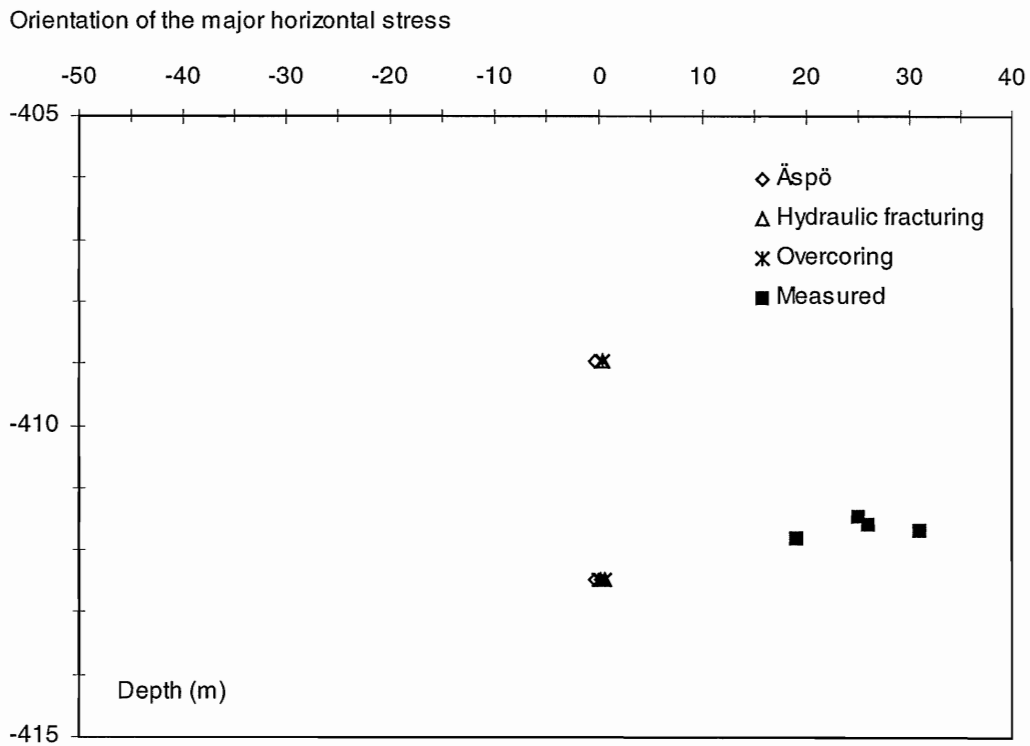
Figure 5-14. *The orientation of the major horizontal stress in the horizontal borehole KXZSD8HL.*

51
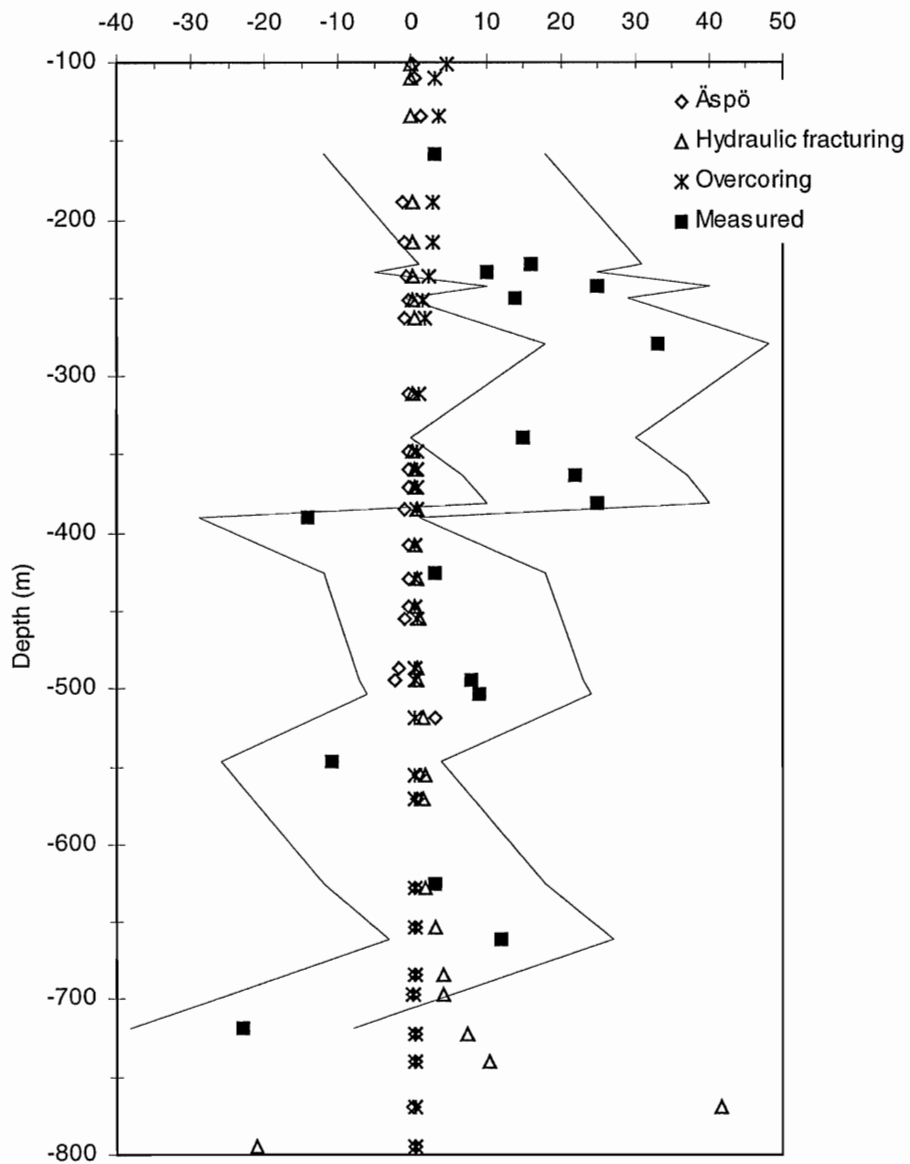
Figure 5-15. *Orientation of the major horizontal stress in KAS02.*
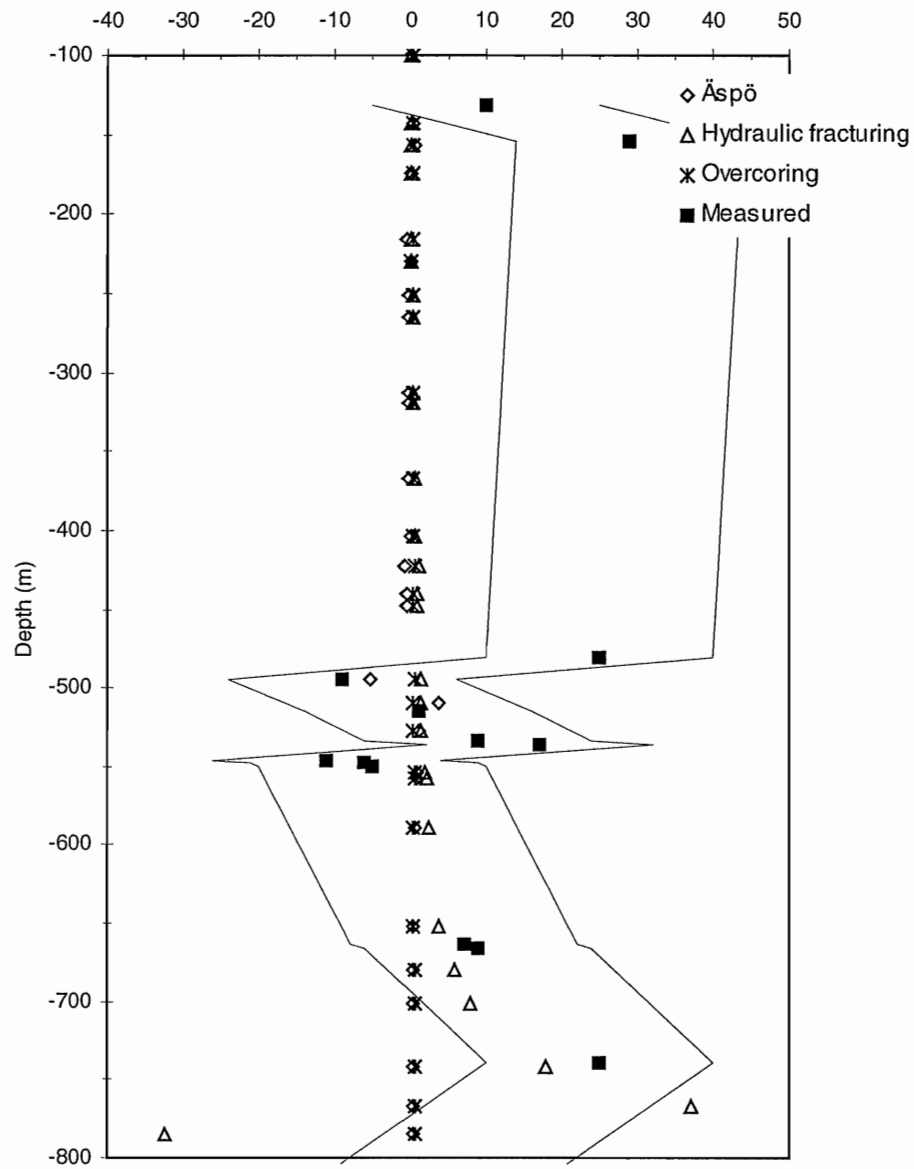
Figure 5-16. *The orientation of the major horizontal stress in KAS03.*
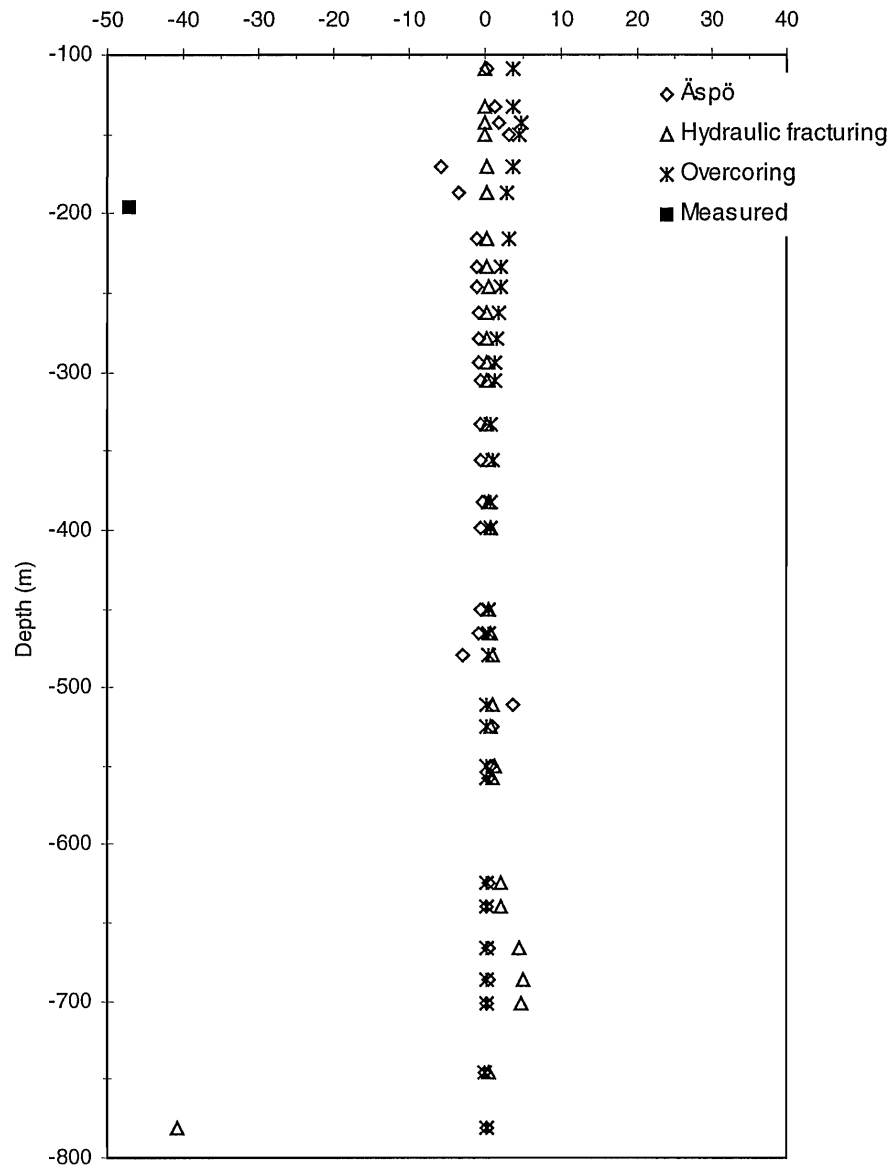
Figure 5-17. *The strike of the major horizontal stress in KAS05.*

5.8   Discussion

The bilinear state of stress gave a better agreement with the measured stresses than the other two, mainly because this state of stress is obtained from the actual measurements at Äspö. However, it does not correlate to 100 %, which would have been unlikely. The measured stresses are influenced, not only by the major discontinuities, but also by the regional and local structures. The proposed bilinear virgin state of stress is, however, also a gross simplification, which is obvious from Figure 5-18.
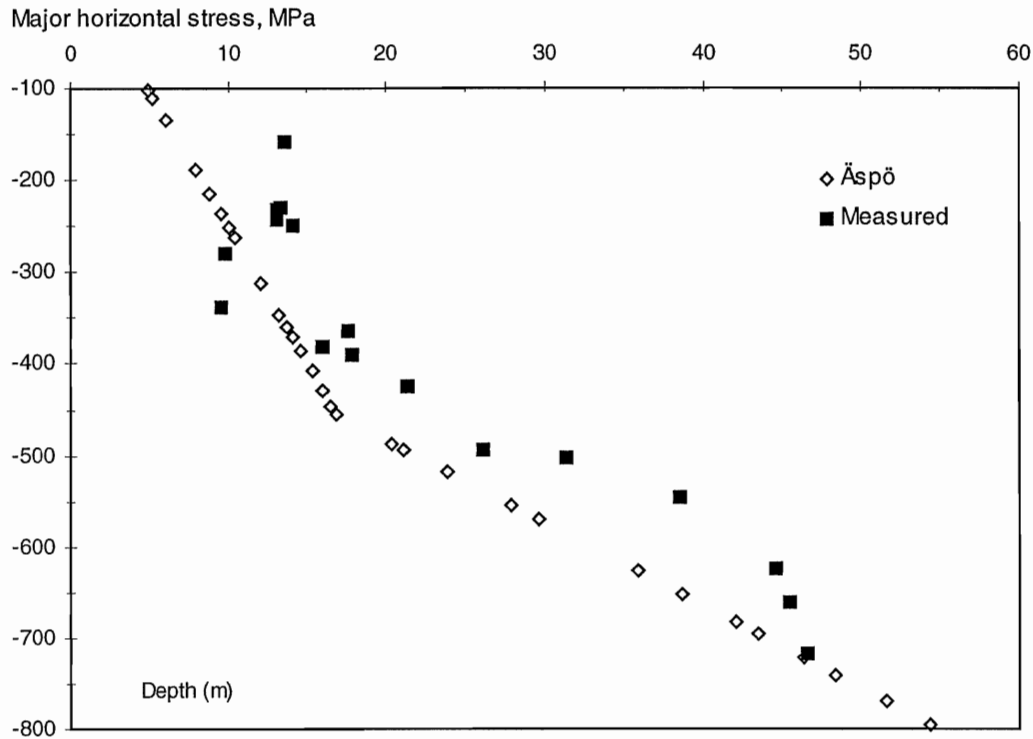
Figure 5-18.   *The measured rock stress at Äspö and the stresses achieved from the bilinear virgin state of stress in KAS03.*

6 Summary and Recommendation

6.1 Geology at Äspö

During this work, no mapping of the rock mass or the discontinuities has been done. Therefore, all the information of the discontinuities and the rock mass has been gathered from a large number of reports. In some cases information regarding the same discontinuity can be different in different reports. To avoid error, communication has been held with SKB to gain approval of the chosen information. The mylonite zones detected by Wikman et al. (1988) is obviously not defined as a major discontinuity since it is not included in the reports defining the major structures at Äspö.

In order to achieve results within a reasonable calculation time, only the major discontinuities at Äspö were included in the analyses.

The orientation of the maximum horizontal stress and the trend interval of all the steeply dipping fractures found at Äspö (ZEDEX, 1996) show a relative good agreement, indicating that the stresses have had a great influence on the fracture propagation or vice versa.

6.2 FLAC analyses

FLAC models were used to analyse the stresses and strains during overcoring and biaxial testing. The results from the overcoring simulation showed that an extensional strain of about 300 microstrain ($\mu\varepsilon$) may occur when the major principal stress is perpendicular to the borehole axis. Since the critical strain in granite is about 250 $\mu\varepsilon$, the extensional strains may induce microcracks in the core. When the major principal stress is parallel to the borehole axis, the largest extensional strains became 150 $\mu\varepsilon$.

When microcracks are initiated and propagated in the core during overcoring, the estimated stresses may deviate from their true values since the measured strains also include opening of and/or sliding along small cracks. On the other hand, if the microcracks are opened or propagated during the biaxial test, this may result in a high Poisson's ratio and then introduce error in the transformation from strains to stresses.

6.3 UDEC analyses

The 2-dimensional conceptual models studied with *UDEC* including a single discontinuity were made to improve the understanding of the influence of discontinuity properties on the state of stress.

An inclined discontinuity affects the magnitude as well as the orientation of the major principal stress in the model, especially if slip occurs along the discontinuity. Therefore, the combination of dip angle and friction angle of the discontinuity will govern the behaviour. .

A thick zone with high strength contacts resulted in a disturbance of the stresses mainly within the zone. The stresses in the host rock showed almost no disturbance due to the zone. The same phenomenon is true for the orientation of the major principal stress, where it is mainly affected within the zone. The influence of Young's modulus, Poisson's ratio and density of the zone on the state of stress was studied. Both Young's modulus and Poisson's ratio affected the magnitude and the orientation of the principal

stresses. If the elastic properties, E and ν, of the zone material were higher than those for the side rock, the magnitude of the stresses were higher within the zone than outside. The orientation of the major principal stress becomes more perpendicular to the zone as well. The density of the zone material did not affect the magnitude or the orientation of the principal stresses.

The results show that whether a zone with low strength contacts or a single discontinuity with low strength contacts are analysed the stresses were affected in affected in the vicinity of the discontinuity exactly the same. However, the magnitudes of the stresses were not sensitive to the normal and shear stiffness of the discontinuity or contact (i.e. a 5-meter thick zone showed almost the same stress magnitudes as a 100-meter thick zone). The orientation of the major principal stress was not affected much, about 10 degrees from the horizontal.

The diagrams over the different stress ratios show that the stresses are affected several hundreds of meters above and below the discontinuity compared to a model without a discontinuity. However, larger change in magnitudes of the principal stresses occurs very close to the discontinuity. Taking this into consideration regarding the stress measurements in the field, a discontinuity can be found if measurements are made on both sides of it. Unfortunately, to say anything about the size of the discontinuity i.e. the extension of the discontinuity, will be difficult. However, the zone of disturbance must be related to the length and the shear strength of the discontinuity. Still, the stress measurement techniques (overcoring and hydraulic fracturing) are said to measure the stress in a block volume of cm^3 - m^3 size. If there is a local discontinuity it can affect the measurement at this location. Taking all the stress measurement results together and studying them in a larger regional scale, the influence of the local discontinuities may only generate a scatter while the larger discontinuities may give rise to regional disturbances. Using a finer mesh near the discontinuity, the stress changes (both magnitudes and orientation) in the absolute vicinity of the discontinuity could be detected. In the models analysed, the closes point to measure the stress magnitudes and orientation is about 10 metres, which may be to large in order to observe the changes close to the discontinuity. However, increasing the mesh density will increase the computer time considerably.

6.4   3DEC analyses

The 3-dimensional model in *3DEC* was made to find out if there is any correlation between measured stresses and the major geological structures at Äspö. Unfortunately, none of the tested stress states coincide with the measured rock stress in the analysed boreholes. The bilinear stress state that was based on a number of rock stresses measurements from Äspö agreed best with the measured rock stresses.

However, these analyses showed how difficult it is to illustrate the complex reality with a simplified model. Even in a large scale, only to identify the overall stresses, many parameters influence the rock stresses.

Finally, since rock stress measurements are made in a point the magnitudes and the orientation depends on both local a regional conditions. It is not so easy that the larger discontinuities themselves cause all the disturbances. The minor discontinuities and heterogeneity of the rock mass also influence and causes disturbances on the rock stresses see Figure 6-1.
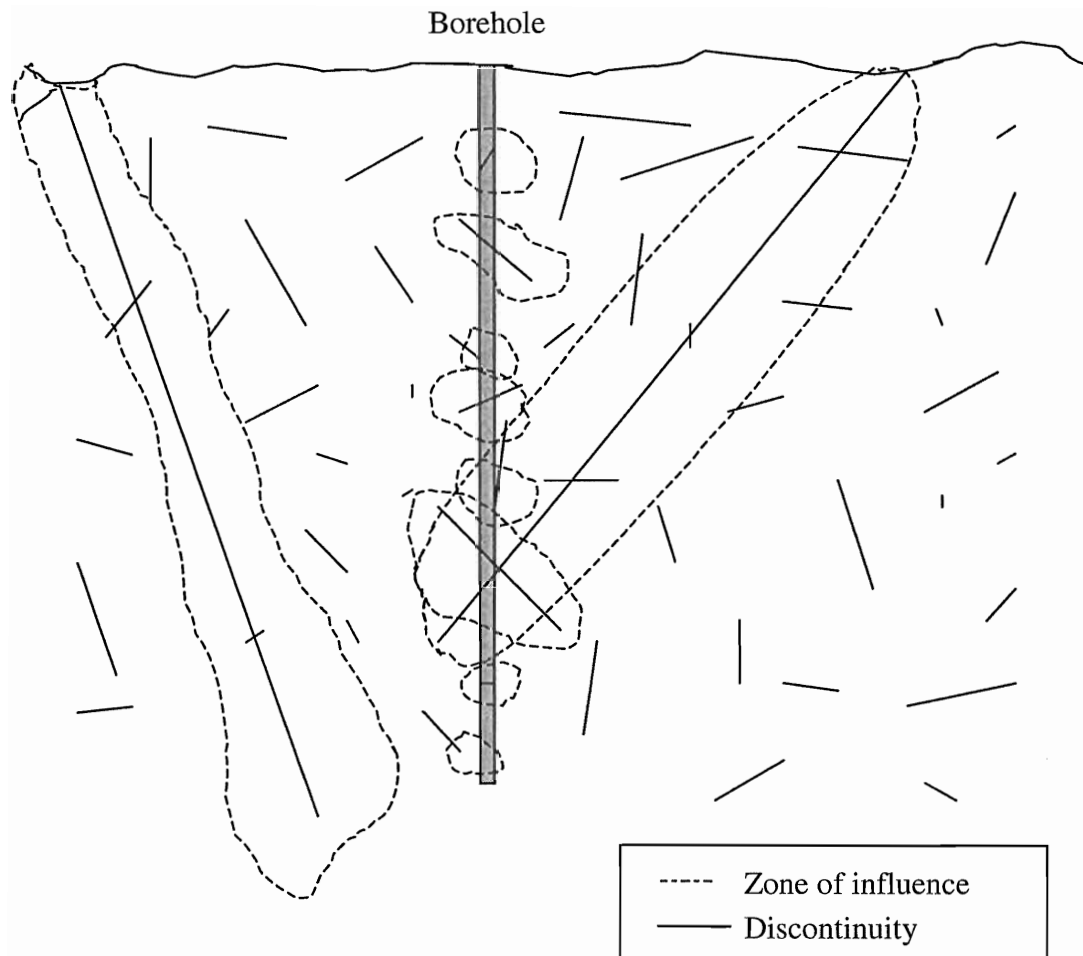
Figure 6-1. *A schematic figure of the causes to disturbances on the rock stresses along a borehole.*

6.5   Suggestions for further work

The numerical modelling of the overcoring and biaxial testing in *FLAC* showed that extensional strain occurs when the major principal stress is perpendicular to the borehole axis. Therefore, it should be interesting to study cores from the field and if possible cores from the measurement points in KA3579G at Äspö. By studying the thin sections in the microscope the results from the numerical modelling could be supported by the results from the microscopic study with reference to the presence of microcracks.

Another approach to interpret the results from the rock stress measurement along a pre-investigation borehole could be to conduct measurements by geophysical methods in the same borehole. Measuring While Drilling (MVD) might also be an approach to obtain information about the rock along the actual borehole. Both these approaches could be a contribution to interpret the rock stresses at the pre-investigation phase of a site.

References

Amadei, B. and Stephansson, O. (1997). *Rock stress and its measurement.* Chapman & Hall, Cambridge.

Barton, N. (1973), A review of the shear strength of filled discontinuities in rock In: Fjellsprengningstekinikk, bergmekanikk, geoteknikk, Oslo, 1973, Tapir Press, Trondheim.

Bjarnason, B., Klasson, H., Leijon, B., Strindell, L. And Öhman, T., (1989). *Rock Stress Measurements in Boreholes KAS02, KAS03 and KAS05 on Äspö.* SKB Progress Report 25-89-17.

Hakami, E., Olofsson, S. -O., Hakami, H. and Israelsson, J., (1998). *Global thermo-mechanical effects from a KBS-3 type repository - Summary report.* SKB Technical Report 98-01.

Hudson, J. A. and Cooling, C. M., (1988). *In-situ* rock stresses and their Measurement in the U.K. – Part I. The current state of knowledge. *Int. J. Rock Mech. Min. Sci. & Geomech. Abstr.* Vol. 25, No 6, pp. 363–370.

Itasca Consulting Group, (1996). *UDEC version 3.00 - User's Manual.*

Itasca Consulting Group, (1998a). FLAC *version 3.40 - User's Manual.*

Itasca Consulting Group, (1998b). *3DEC version 2.00 - User's Manual.*

Lee, M. Hewitt, T. and Stillborg, B. (1994*). Äspö Virgin Stress Measurement Results - Measurements in Boreholes KA1899A, KA2198A and KA2510A.* SKB Technical Note 25-94-13V.

Lee, M., Bridges, M. and Stillborg, B., (1993), *Äspö Virgin Stress Measurements Results in Section 1050, 1190 and 1620 m of the Access Ramp,* SKB Progress report 25-93-02.

Litterbach, N., Lee, M., Struthers, M. and Stillborg, B., (1994), *Virgin Stress Measurement Results Boreholes KA2870A and KA3068A,* SKB Progress report 25-94-32.

Ljunggren and Klasson, H. (1996*). Rock Stress Measurements at the ZEDEX Test Area, Äspö HRL.* ÄSPÖ HRL Technical Note TN-96-08z.

Ljunggren, C. and Bergsten, K-Å., (1998), *Rock stress measurements in KA3579G,* SKB Progress report HRL-98-09.

Lundholm, B., (2000). *Rock stress and Rock Stress Measurements at Äspö.* SKB IPR-00-24.

Martin, C.D. and Christiansson, R., (1991). Overcoring in Highly Stressed Granite - the Influence of Microcracking. *Int. J. Rock Mech. Min. Sci. & Geomech. Abstr.* Vol. 28, No 1, pp. 53-70.

Rhen, I., Bäckbom, G., Gustafsson, G., Stanfors, R. and Wikberg, P., (1997a). *ÄSPÖ HRL - Geoscientific evaluation 1997/2. Results from pre-investigations and detailed site characterisation. Summary report.* SKB TR 97-03.

Rhén, I., Gustavsson, G., Stanfors, R. and Wikberg, P., (1997b). *ÄSPÖ HRL – Geoscientific evaluation 1997/5. Models based on site characterization 1986-1995.* SKB TR 97-06.

Spiegel, M. R. (1968). *Mathematical Handbook of Formulas and Tables.* Schaum's Outline Series, McGraw-Hill Book Company.

Stacey, P., (1982). Contribution to the mechanism of core discing. *Journal of the South African Institute of Mining and Metallurgy.* Vol. 82, 269-274.

Stacey, T. R. & Page, C. H., (1986). *Practical Handbook for Underground Rock Mechanics.* Trans Tech Publications, Germany.

Stacey, T. R., (1981). A simple Extension Strain Criterion for Fracture of Brittle Rock. *Int. J. Rock Mech. Min. Sci. & Geomech. Abstr.* Vol. 18, pp. 469-474.

Stanfors, R., Olsson, P. and Stille, H., (1997). *ÄSPÖ HRL - Geoscientific evaluation 1997/3. Results from pre-investigations and detailed site characterisation. Comparison of predictions and observations. Geology and mechanical stability.* SKB TR 97-04.

Stenberg, L., (2000). *Personal communication.* SKB Äspö.

Stille H. and Olsson, P., (1996). *Summary of mechanical experience from the construction of Äspö Hard Rock Laboratory.* SKB PR HRL-96-07.

Appendix A

Table A-1. Results from rock stress measurements in KAS02.

Number	Depth (m)	σ_{HI}	σ_{HII}	σ_h	Bearing of σ_H	σ_{HII}/σ_h
1	113	7.5	6.0	4.7	-	1.28
2	159	13.6	10.2	5.9	138	1.73
3	229	13.3	10.3	5.5	151	1.87
4	233	13.0	10.3	5.2	145	1.98
5	243	13.0	9.5	5.4	160	1.76
6	250	14.0	10.9	5.9	149	1.85
7	280	9.8	9.1	5.2	168	1.75
8	339	9.6	10.2	5.7	150	1.79
9	364	17.6	10.7	6.6	157	1.62
10	381	16.0	12.3	6.8	160	1.81
11	390	17.8	12.8	7.0	121	1.83
12	426	21.4	17.2	8.8	138	1.95
13	495	26.1	22.9	13.7	143	1.67
14	504	31.4	27.8	16.0	144	1.74
15	515	27.1	23.5	12.6	-	1.87
16	547	38.5	35.1	19.0	124	1.85
17	585	46.1	43.9	23.9	-	1.84
18	625	44.5	41.4	23.0	138	1.8
19	661	45.4	39.9	22.4	147	1.78
20	718	46.6	42.5	24.4	112	1.74
21	737	42.9	40.5	21.0	-	1.93

Table A-2. Rock stress measurements in KAS03.

Number	Depth (m)	σ_{HI}	σ_{HII}	σ_h	Bearing of σ_H	σ_{HII}/σ_h
1	131.5	5.7	5.0	3.6	145	1.39
2	153.8	4.3	6.8	4.5	164	1.51
3	347.4	-	-	-	Horizontal fracture	
4	481.4	19.8	19.5	10.7	160	1.82
5	494.8	22.4	20.7	10.9	126	1.90
6	515.1	20.8	19.4	11.8	136	1.64
7	534.0	26.7	25.1	11.8	144	2.13
8	536.0	25.6	24.4	12.4	152	1.97
9	545.9	21.8	20.2	10.7	124	1.89
10	547.9	1.9	17.7	9.8	129	1.81
11	550.9	19.3	18.0	9.8	130	1.84
12	625.3	19.9	18.3	10.0	-	1.83
13	664.0	18.3	15.1	8.5	142	1.78
14	666.0	22.5	18.8	9.6	144	1.96
15	739.4	33.8	26.1	13.7	160	1.91
16	819.8	44.2	37.9	22.6	-	1.68
17	822.3	43.4	43.7	23.0	-	1.9
18	877.4	40.7	38.5	21.0	-	1.83
19	880.4	40.1	39.5	21.4	118	1.85
20	885.4	45.7	43.0	22.6	157	1.9
21	893.3	47.2	46.3	24.3	-	1.91
22	962.8	48.0	48.5	24.9	115	1.95

Table A-3.   Rock stress measurements in KAS05.

Nr	Depth	E	ν	σ_1	Dip dir.	Dip	σ_2	Dip dir.	Dip	σ_3	Dip dir.	Dip
1	195.31	58	0.20	10.3	268.0	13.9	2.4	0.4	9.4	1.5	123.4	73.2
2	196.61	63	0.25	10.2	234.1	23.8	7.9	137.9	13.8	3.9	20.3	62.0
3	197.41	64	0.13	13.4	273.1	17.4	8.4	64.3	70.3	4.9	180.3	8.9
4	355.01	74	0.22	20.2	261.6	43.4	14.4	123.6	38.1	-0.7	14.7	22.5
5	355.91	68	0.19	16.2	86.8	76.2	10.1	305.0	10.9	-3.0	213.4	8.3
6	356.81	62	0.16	10.8	281.4	10.9	5.4	135.1	77.0	-0.7	12.8	7.0
7	357.74	68	0.19	17.7	102.9	2.7	4.9	201.3	71.9	2.1	12.0	17.8

Table A-4.   Rock stress measurements from KXZSDS8HL.

Nr	Depth	E	ν	σ_1	Dip dir.	Dip	σ_2	Dip dir.	Dip	σ_3	Dip dir.	Dip
1	21.81	Borre did not release from adapter										
2	23.37	70	0.30	18.3	337	35	9.6	212	39	5.1	92	32
3	24.06	65	0.30	19.7	357	19	9.1	262	16	7.2	134	65
4	24.75	66	0.25	20.2	351	20	9.1	220	61	5.9	89	20
5	25.44	66	0.26	23.2	355	25	12.1	104	35	9.2	238	44